Lawrence Berkeley National Laboratory
LBL Publications

Title

Rates and multiple sulfur isotope fractionations associated with the oxidation of sulfide by oxygen in aqueous solution

Permalink

https://escholarship.org/uc/item/28x886fv

Authors

Eldridge, Daniel L

Farquhar, James

Publication Date

2018-09-01

DOI

10.1016/j.gca.2018.06.030

Peer reviewed

Rates and multiple sulfur isotope fractionations associated with the oxidation of sulfide by oxygen in aqueous solution

Daniel L. Eldridge *, James Farquhar

Department of Geology and ESSIC, University of Maryland, College Park, MD 20740, United States

Received 2 February 2018; accepted in revised form 22 June 2018; Available online 30 June 2018

Abstract

Sulfide oxidation is a major component of the global sulfur cycle that requires consideration in isotope-based models of aquatic and sedimentary systems, but the isotope fractionations based on analyses of all three isotope ratios of sulfur ($^{33}S/^{32}S$, $^{34}S/^{32}S$, $^{36}S/^{32}S$) have yet to be documented for abiological sulfide oxidation processes. We present experimental determinations of the reaction rates and sulfur isotope fractionations associated with the oxidation of aqueous sulfide (principally HS^-) by molecular oxygen ('autoxidation') in high pH ($\approx$9.8), low ionic strength carbonate/bicarbonate buffered solutions as a function of temperature (5–45 °C) and trace metal catalysis (ferrous iron, added $[Fe^{2+}] \sim$50–150 nM). Rates and isotope fractionations are quantified *via* the analysis of sulfide as a function of reaction progress over relatively low extents of reaction (ca. 33–47%). The oxidation of sulfide at pH = 9.8 and 25 °C without any catalyst added is associated with a computed second order rate constant (k) of $\ln k = 3.49 \pm 0.38$ (k in $M^{-1} hr^{-1}$; 2 s.d., quadruple experiments) and major sulfur isotope discrimination of $^{34}\varepsilon_{P-R} = -5.85 \pm 0.43$‰ (2 s.d., duplicate experiments) that are both consistent with previous studies, and a corresponding minor sulfur isotope fractionation relationship of $^{33/34}\theta = 0.509 \pm 0.004$ that translates to $\Delta^{33}S_{P-R} = 0.033 \pm 0.018$‰ (2 s.d.). The dependence of $^{34}\varepsilon_{P-R}$ on reaction rate due to either temperature or ferrous iron catalysis over the ranges we have studied is small ($<\sim$1‰ in $^{34}\varepsilon_{P-R}$) and similar values for $^{33/34}\theta$ and $\Delta^{33}S_{P-R}$ are obtained for all conditions studied (e.g., mean of all 7 experiments: $^{33/34}\theta = 0.5082 \pm 0.0031$ and $\Delta^{33}S_{P-R} = 0.037 \pm 0.014$‰; 2 s.d.). These results indicate that the process of sulfide autoxidation has a mass dependence that is resolvable from the expectations of typical equilibrium isotope exchange. Values for $^{36/34}\theta$ and $\Delta^{36}S_{P-R}$ may also exhibit deviations from typical equilibrium isotope exchange but are not resolved under all conditions studied. The shift in values of $^{33/34}\theta$ and $\Delta^{33}S$ (and potentially $^{36/34}\theta$ and $\Delta^{36}S$) is consistent with the hypotheses that kinetic isotope effects can be associated with different mass laws than equilibrium processes or with reversibility occurring in the initial parts of the reaction network leading to oxidation products, but both hypotheses will likely require further investigation. We provide an example of how our experimentally calibrated 'signature' for sulfide autoxidation may be identified in natural data using the previously published $\delta^{34}S$ and $\Delta^{33}S$ values of dissolved sulfide in proximity to the oxic-sulfidic interface in the water column of the Cariaco Basin. The observation that the autoxidation of aqueous sulfide in high pH media is associated with a non-zero $\Delta^{33}S_{P-R}$ will influence how chemical oxidation processes are treated in environmental and global scale models of the sulfur cycle based on multiple sulfur isotopes.
© 2018 Elsevier Ltd. All rights reserved.

1. INTRODUCTION

Sulfide oxidation processes are major components of the low temperature cycling of sulfur and other key elements (e.g., O, C, N, Fe, Mn, etc.) in Earth surface environments. The oxidative weathering of sulfide minerals in the Earth's

* Corresponding author at: Geophysical Laboratory, Carnegie Institution of Washington, 5251 Broad Branch Road NW, Washington, DC 20015, United States.
  E-mail address: deldridge@carnegiescience.edu (D.L. Eldridge).

crust is ultimately responsible for the accumulation of sulfate in the global oceans over geological timescales, and this sulfate fuels anaerobic respiration in the form of microbial sulfate reduction (MSR; or dissimilatory sulfate reduction) in organic-rich marine sedimentary environments. Due to the high abundance of sulfate in the modern oceans ($\sim$0.03 mol/kg), MSR accounts for a significant proportion of the organic carbon respiration budget that globally may amount to $\sim$12–29% of the total respiration of the organic carbon flux to the seafloor per year (Bowles et al., 2014), and can account for upwards of 50% of the total organic matter respired in localized shelf sediments (e.g., Jørgensen, 1982). The copious amounts of aqueous sulfide produced by anaerobic respiration *via* sulfate reduction may undergo further re-oxidation or be sequestered as authigenic sulfide minerals (e.g., pyrite) or in organics (*via* sulfurization), where the relative balance between sulfide oxidation processes and pyrite burial have significant consequences for the abundance of O_2 in Earth's surface environment over geologic timescales. From studies of modern coastal marine sediments, an estimated ca. 80–95% of the sulfide generated by MSR is re-oxidized ultimately back to sulfate (Jørgensen, 1977; Jørgensen, 1982; Jørgensen et al., 1990; Canfield and Teske, 1996; Jørgensen and Nelson, 2004). Thus, sulfide re-oxidation processes are major features of the global geochemical cycle due in part to the availability of oxidants in the modern ocean, and can involve numerous abiological and biological pathways tied to numerous oxidants/terminal electron acceptors (e.g., O_2, MnO_2, Fe-oxyhydroxides, and NO_3^- that represents a pathway of denitrification). Sulfide oxidation processes therefore warrant detailed inclusion into considerations of isotope-based models of the sulfur cycle.

Despite the importance and ubiquity of oxidative sulfur cycling, experimental constraints on the sulfur isotope fractionations based on $^{33}S/^{32}S$, $^{34}S/^{32}S$, and $^{36}S/^{32}S$ are minimal for sulfide oxidation processes and, thus, sulfide oxidation is incompletely treated in current models of the sulfur cycle. The existing constraints are biological and comprise experimental studies performed with the anaerobic phototrophic green sulfur bacterium *Chlorobium tepidum* (Zerkle et al., 2009), and studies of natural samples associated with microbial mats that are attributed to the activities of natural populations of chemotrophic sulfide oxidizing bacteria (Zerkle et al., 2016). Substantial oxidative cycling of sulfide occurs by way of abiotic chemical pathways in natural environments that result from mechanisms that are independent from intracellular enzyme-mediated pathways that can result in different isotope fractionations. The valuable and existing calibrations of sulfur isotope fractionations accompanying the abiological oxidation of aqueous sulfide (H_2S/HS^-) by molecular oxygen (O_2; 'autoxidation' herein) provided by Fry et al. (1988) pre-date the more recent emphasis on the analysis of minor sulfur isotopes ($^{33}S/^{32}S$, $^{36}S/^{32}S$) and require a re-examination for future environmental applications. Due to the paucity of constraints, most isotope-based models of the environmental sulfur cycle to date contain the assumption that sulfide autoxidation is associated with a mass dependence that conforms to equilibrium isotope exchange (i.e., $^{33/34}\theta = 0.515$ and $\Delta^{33}S_{products-sulfide} = 0\%o$; definitions of these variables are given in Section 2.5).

The rates and isotope fractionations associated with a unidirectional process such as the autoxidation of aqueous sulfide are intimate expressions of the reaction mechanism, and studies examining the isotope fractionations of autoxidation should therefore include a concomitant examination of rates for interpretive context. Numerous experimental studies have investigated the rates of sulfide autoxidation in relatively low-ionic strength experimental buffer solutions (Avrahami and Golding, 1968; Millero et al., 1987; Chen and Morris, 1972a; O'Brien and Birkner, 1977; Luther et al., 2011) and seawater (Ostlund and Alexander, 1963; Cline and Richards, 1969; Almgren and Hagstrom, 1974; Millero et al., 1987; Zhang and Millero, 1993a). The reaction has also been studied as a function of various catalysts including trace metals (e.g., Chen and Morris, 1972b; Hoffmann and Lim, 1979; Vazquez et al., 1989; Zhang and Millero, 1993a) and organic compounds (Chen and Morris, 1972b). The rate of sulfide oxidation is understood to follow a general rate law:

$$-\frac{d\left[(H_2S)_T\right]}{dt} = k\left[(H_2S)_T\right]^a[O_2]^b \tag{1}$$

where $(H_2S)_T$ refers to the sum of all aqueous sulfide species (H_2S, HS^-, S^{2-}) under a given set of conditions, brackets ('[]') denote concentrations, k is the overall rate constant, and 'a' and 'b' denote the reaction order with respect to sulfide and oxygen, respectively. The overall rate constant is a function of temperature, pH, and ionic strength (Millero et al., 1987), and the reaction orders with respect to sulfide and oxygen are interpreted in terms of the stoichiometry of the rate determining step(s) in the reaction and are quantified experimentally.

Rate law parameters (k, a, and b) from previous experimental studies are summarized in Table 1. It is generally agreed that aqueous sulfide autoxidation follows a second order rate law overall where the reaction orders with respect to sulfide and oxygen are both unity (Table 1), with few exceptions (Chen and Morris, 1972a) that have not been reproduced by subsequent experimentation (*cf.* O'Brien and Birkner, 1977; Millero et al., 1987; Zhang and Millero, 1993a). However, second order rate constants derived from experiments performed under comparable conditions vary significantly between laboratories (Table 1; see also reviews in Millero, 1986; Millero et al., 1987; Zhang and Millero, 1993a). For example, the estimated half-times ($t_{1/2}$) of sulfide disappearance in high pH, air-saturated, and low ionic strength buffer solutions derived from literature second order rate constants range from 6 h (Avrahami and Golding, 1968) to 397 h (Luther et al., 2011) at 25 °C (Table 1). Among the simplest and most often suggested hypotheses for this apparent inter-laboratory variability is varying degrees of unintentional background trace metal catalysis (e.g., Millero, 1986; Zhang and Millero, 1993a; Luther et al., 2011). This hypothesis is supported by the observation that apparent second order rate constants can vary by several orders of magnitude as a result of trace metal catalysis under otherwise equivalent solution conditions (e.g., Vazquez et al., 1989; Zhang and Millero,

Table 1

Conditions and rate law parameters from experimental studies of sulfide oxidation via molecular oxygen, where $-d[(H_2S)_T]/dt = k[(H_2S)_T]^a[O_2]^b$. The solution medium "w" ("water") refers to low ionic strength buffer solutions, and "sw" refers to seawater (with reported salinity, when available). Millero et al. (1987) provide evidence that the rates of sulfide oxidation are uniform within reasonable experimental uncertainty over pH ranges where a singular sulfide species is present (i.e., HS^- or H_2S), thus differences in rate law parameters above a pH of ~8 over the tabulated ranges are not expected to be major when solution conditions are otherwise comparable. The values of 'b' in parentheses indicate the values assumed by the original authors where applicable. The column $\ln k$ represent the second order (a = 1, b = 1) rate constant either as reported in the reference or computed here (units: $M^{-1} hr^{-1}$). The half-time of sulfide disappearance ($t_{1/2}$) is computed for 25 °C experiments assuming $[O_2] = 250$ μM, and is reported in units of hours.

Reference	Medium	T (°C)	pH	a	b	$\ln k$	$t_{1/2}$
Avrahami and Golding (1968)	w	25	12	1	n.d.	5.3	14
	w	25	14	1	n.d.	6.2	6
Chen and Morris (1972a, 1972b)	w	25		1.34	0.56	N/A	N/A
O'Brien and Birkner (1977)	w	25	10	1	0.80 ± 0.25 (1)	4.9	21
Millero et al. (1987)	w	25	8.0	1	n.d. (1)	4.3 ± 0.6	44 ± 30
Zhang and Millero (1993a, 1993b)	w	25	8.2	1	1	3.75	65
Luther et al. (2011)	w	25	12	1	n.d. (1)	1.94 ± 0.05	397
Millero et al. (1987)	sw (S = 35)	25	8.0	1	n.d. (1)	5.2 ± 0.6	16 ± 9
Zhang and Millero (1993a, 1993b)	sw (S = 35)	25	8.2	1	1	4.81 ± 0.02	23
Cline and Richards (1969)	sw	9.8	7.5–7.8	1	1	~6.9	N/A

1993a), and by the results from recent experiments performed under 'trace metal clean' conditions that yield the lowest second order rate constants to date for sulfide autoxidation (Luther et al., 2011; Table 1). The issue of contaminating trace catalysts may therefore complicate the calibration of rates and isotope fractionations in the laboratory and may underscore the need to quantify rates in addition to fractionation factors in experimental studies of sulfide autoxidation.

We present experimental determinations of the reaction rates and sulfur isotope fractionations associated with the chemical oxidation of aqueous sulfide (principally HS^-) via molecular oxygen in high pH, low ionic strength carbonate/bicarbonate buffered solutions as a function of temperature (5–45 °C) and trace metal catalysis (ferrous iron, Fe^{2+}, ~50–150 nM). Ferrous iron is chosen to explore catalytic effects because it appears to be one of the most sensitive, impactful, and environmentally relevant catalysts for aqueous sulfide oxidation in relatively high pH solutions (Vazquez et al., 1989; Millero, 1991a–c; Zhang and Millero, 1993a). The approach of measuring reaction rates in addition to isotope fractionations allows for the exploration of any potential relationships between the two variables, and also allows us to place our experiments in the context of the extensive experimental kinetics literature (e.g., Avrahami and Golding, 1968; Chen and Morris, 1972a, 1972b; O'Brien and Birkner, 1977; Millero et al., 1987; Zhang and Millero, 1993a; Luther et al., 2011). Rates and isotope fractionations are estimated via the analysis of the concentration and isotopic composition of sulfide as a function of reaction progress. The low concentrations of intermediates/products (e.g., SO_3^{2-}, $S_2O_3^{2-}$, SO_4^{2-}) prevented their isotopic analysis, and these remain targets for future studies. Despite these limitations, the present study presents the first high-precision multiple sulfur isotope analyses that constrain how the isotopic composition of sulfide (comprised principally of HS^-) may evolve as a result of, and be affected by, the process of autoxidation under environmentally relevant conditions, and represent key

constraints for understanding data from natural systems and informing future environmental models of the sulfur cycle based on multiple sulfur isotope ratios.

2. METHODS

2.1. Reaction vessel + solution, and chemical assays

The reaction vessel and its cleaning protocol were carefully chosen to minimize the introduction of trace metal catalysts into our reaction solutions. Our reactor consists of all plastic and/or Teflon components: a polypropylene bottle (2 L, Nalgene) fitted with a 2–3 port Teflon-seal and gasket cap (Vaplock), Teflon magnetic stir bar, and 1/8" OD PEEK tubing submerged in the reaction solution for aliquot time series sampling for concentration and isotopic analyses. Aliquot sampling is performed by peristaltic pump. All components are acid-soaked (6 M HCl) for several weeks followed by a Milli-Q soak of comparable duration, and subsequently rinsed several times with Milli-Q prior to loading of reaction solution. The use of plastics/Teflon and extensive acid cleaning is employed to minimize trace metal contamination that could affect the rates and observed isotopic fractionations (cf. Vazquez et al., 1989; Luther et al., 2011). Measurements of pH were made on aliquots removed from the reaction vessel rather than by direct submersion in the reaction solution to avoid any potential catalytic effects of the probe. Reaction solutions were actively stirred throughout experimental runs utilizing a Teflon magnetic stir bar, and roughly half the volume of the reaction vessel is air-headspace by design to enhance air-solution gas exchange. Temperature control is achieved by the submersion of reaction vessels in a circulated VWR temperature bath (Model 1186D; stable to 0.01 °C).

Reaction solutions are buffered to a pH that simplifies the aqueous speciation of sulfide to the anionic form (HS^-) in order to avoid loss of the volatile H_2S species that could convolute our analysis. Reaction solutions are comprised of 1 L Milli-Q buffered with $NaHCO_3/Na_2CO_3$

(0.002–0.02 M) to a pH of ~9.8. Buffer solutions were prepared using acid-cleaned volumetric flasks (Nalgene, polypropylene, 1 L) following the cleaning protocol for the reaction vessel and using reagent grade Na_2CO_3 and $NaHCO_3$ (Sigma Aldrich: ≥99.5% Na_2CO_3 and 99.7–100.3% $NaHCO_3$). Bicarbonate/carbonate buffers were chosen due to their relevance in buffering many natural systems. Under these conditions, the speciation of sulfide is overwhelmingly in the anionic form of HS^- (~100% HS^-; Hershey et al., 1988). Conditions were chosen to minimize $H_2S_{(aq)}$ in solution to prevent a substantial vapor pressure of $H_2S_{(g)}$, which could lead to sulfide loss from solution and confound the rate and isotope fractionation determination. Prior to sulfide injection, reaction solutions are allowed to thermally equilibrate in the temperature bath overnight. The following morning, reaction solutions are bubbled for one hour with ambient air using the peristaltic pump immediately prior to sulfide injection in an attempt to guarantee reaction solutions are saturated with respect to O_2 at the beginning of the experiment (after Millero et al., 1987).

Small aliquots of freshly prepared stock sulfide solutions were injected into the reaction vessel to initiate the experiment. Stock sulfide solutions were prepared from sodium sulfide nonahydrate crystals ($Na_2S \cdot 9H_2O$; J.T. Baker, 101.3%) stored at −20 °C and rinsed in N_2-purged Milli-Q and patted dry with Kimwipes prior to weighing. Fresh stocks of sodium sulfide were prepared for every experiment by dissolving rinsed and dried crystals in small concentrated batches (~5 ml, ~0.2 M) in acid cleaned polypropylene VWR centrifuge tubes under an anoxic N_2:H_2 atmosphere (95:5%; circulated through palladium catalysts to remove trace O_2) within 30 min of injection into experimental solutions. Aliquots of these stock sulfide solutions (1 ml; ~0.2 M) were injected into experimental solutions using a graduated pipette (Neptune, natural polypropylene tips). Blanks of thiosulfate and sulfite in these stock solutions were typically below the detection limits at the level of dilution in reaction solutions as determined by HPLC (≤0.1 μM) following Zopfi et al. (2004) (see below). For the Fe^{2+}-catalyzed experiments, $FeSO_4$ stock solutions (Sigma Aldrich, ferrous sulfate heptahydrate) were freshly prepared with N_2-purged Milli-Q water under N_2:H_2 (95:5%) atmosphere within 10 min of the beginning of experiments. Aliquots of the freshly prepared ferrous sulfate stock solution (1 ml containing [$FeSO_4$] ≈ 50–150 μM, yielding [$FeSO_4$] ≈ 50–150 nM in reaction solution) were added to experimental solutions immediately following the injection of sulfide. No observed precipitate was observed by eye upon the addition of ferrous iron to experimental sulfide solutions at these low levels.

Concentration analyses of aqueous sulfide were performed via the methylene blue spectrophotometric technique of Cline (1969) and were performed in either duplicate or triplicate for each sampling (reproducibility was typically ≤ 5%, 2 s.d.). Most experiments were designed to have an initial sulfide concentration of around 2.2×10^{-4} M (220 μM), which was chosen as a near-optimal compromise between having sufficient sulfide for isotopic measurement throughout experimental runs (SF_6 GS-IRMS requires about 10–12 μmoles of sulfur for high precision $^{33}S/^{32}S$, $^{34}S/^{32}S$, and $^{36}S/^{32}S$ analysis) and not being so high as to overwhelm the available oxygen supply and, therefore, interfere substantially with the rate analysis based on sulfide disappearance. Oxygen concentrations were estimated under experimental conditions as a function of temperature and ionic strength from previous experimental calibrations (Benson and Krause, 1980, 1984) as implemented in the USGS DOTABLES online software utility (http://water.usgs.gov/software/DOTABLES/). The steps taken to minimize oxygen depletion in the reaction solution as sulfide oxidation proceeded included the vigorous stirring of the reaction vessel via magnetic stir bar, and a voluminous headspace in the reaction vessel that underwent continual ventilation (exchange with ambient air) during aliquot sampling.

The concentrations of sulfite (SO_3^{2-}) and thiosulfate ($S_2O_3^{2-}$ or $S-SO_3^{2-}$) were determined as derivatives of monobromobimane (MBB; i.e., MBB-SO_3 & MBB-S-SO_3) via HPLC with fluorescence detection closely following the protocols of Zopfi et al. (2004). Briefly, 1 ml aliquots of experimental solution were added to 50 μL of acetonitrile containing 0.045 M monobromobimane (Toronto Research Chemicals) and 50 μL of 0.5 M Bicine buffer (pH = 8.0) containing 0.05 M EDTA and allowed to react for 30 min (the derivatization reaction has a half time of about ~7 min). Derivatization was immediately stopped following 30 min via the addition of 50μL of 0.324 M methanesulfonic acid. This acidification step deactivates the monobromomobimane (MBB) and prevents further undesirable side-reactions. Calibrations for sulfite and thiosulfate concentrations were performed using Na_2SO_3 and $Na_2S_2O_3$ stock solutions (reagent grade, Sigma Aldrich; ≥98.0% Na_2SO_3, 99.5% $Na_2S_2O_3 \cdot 5H_2O$) that were prepared and derivatized per protocol above in an anoxic chamber (95:5% N_2:H_2 atmosphere circulated through palladium catalysts). The capability to measure sulfate concentrations was not present in our laboratory during the time of these experiments, and therefore is roughly estimated by difference following the approach of Zhang and Millero (1993a) for their experiments performed in seawater (we refer to this quantity simply as 'remaining S'; Supplementary Material).

Supplementary data associated with this article can be found, in the online version, at https://doi.org/10.1016/j.gca.2018.06.030.

2.2. Kinetics

The experiments are designed after a standard rate law for sulfide oxidation by molecular oxygen (Eq. (1): cf. Millero et al., 1987; Zhang and Millero, 1993a). Following the majority of previous studies and taking the reaction order with respect to sulfide to be unity (Table 1), we took steps to keep O_2 constant described above such that the overall rate law can be simplified to a pseudo-first order rate law:

$$-\frac{d\left[(H_2S)_T\right]}{dt} = k'\left[(H_2S)_T\right]^a \qquad (2)$$

where $k' = k[O_2]^b$ and is referred to as the pseudo-first order reaction constant and can be determined by monitoring sulfide concentration with time *via* the time-integrated and linearized form of the pseudo-first order rate law:

$$\ln\big[(H_2S)_T\big]_t = \ln\big[(H_2S)_T\big]_{t=0} - k't \tag{3}$$

where 't' is time and the subscript 't = 0' denotes the initial concentration of sulfide. The value of k' can be determined *via* the least squares linear regression of sulfide concentration data following Eq. (3). Measured k' can then be computed into the overall rate constant k using the estimated oxygen concentration (and reaction order, 'b') in the experiment. We did not determine the reaction order with respect to oxygen ('b') in our experiments but adopt the reaction order with respect to oxygen from the experiments of Zhang and Millero (1993a), which appear to be among the most reliable and are also consistent with the bulk of the literature observations (Table 1). The reaction is therefore taken to be second order overall ($a + b = 1 + 1 = 2$) and k will be computed and reported in units of M^{-1} hr^{-1} in our study (*cf.* Millero et al., 1987; Zhang and Millero, 1993a; Luther et al., 2011).

2.3. Isotopic analyses of sulfide: SF$_6$ GS-IRMS

Aliquots of experimental solution were extracted throughout experimental runs for the isotopic analysis of residual sulfide to estimate isotope enrichment factors. A total of 5–6 aliquots were extracted from the experimental solution throughout reaction progress removing volumes corresponding to ~10–12 μmoles of sulfide (typically, 60–110 ml of experimental solution), and immediately fixed in an equivalent volume of 200 g/L zinc acetate trapping solution as ZnS and frozen for later processing. The initial processing of sequestered ZnS involves thawing and immediate filtration (0.2 μm, Whatman or Millipore). The filters containing ZnS precipitate are then immediately added to 100 ml round bottom flasks with syringe side arms for routine acid volatile sulfide (AVS) extraction that allows quantitative re-precipitation of sulfide as Ag$_2$S. Briefly, this involves injection of 20 ml of 5 N HCl into the round bottom flask containing the filter + precipitate under flow of N$_2$ through a condenser, water trap, and capture solution (0.02 M AgNO$_3$, 0.2 M HNO$_3$) that quantitatively sequesters the acid-liberated sulfide as Ag$_2$S. Samples of Ag$_2$S were then allowed to settle overnight, after which time they were rinsed in a sequence of Milli-Q, 1 M NH$_4$OH, and Milli-Q (3x each, with centrifugation and vortex mixing) and dried for later fluorinations. Multiple blanks were run on acidified filters following the protocol above and no detectable Ag$_2$S was obtained, indicating that the filter (and reagents) contribute no significant AVS.

Silver sulfide samples were weighed in small aluminum foil envelopes, added to nickel reaction tubes, and reacted in the presence of 100-fold molar excess F$_2$ gas at ~250 °C overnight (12+ hours) to quantitatively convert samples to SF$_6$ gas. The SF$_6$ gas is cryogenically separated from HF and other condensable non-sulfur fluorination byproducts by utilizing a chilled ethanol slurry (−115 °C) before further purification by Gas Chromatography. The yields of this

fluorination, extraction, and SF$_6$ purification were 100% (±5%) for all experimental samples reported herein. The SF$_6$ gas is analyzed for isotope ratios as ion current beams of $^{32}SF_5^+$, $^{33}SF_5^+$, $^{34}SF_5^+$, and $^{36}SF_5^+$ at 127, 128, 129, and 131 mass numbers, respectively, on a ThermoFinnigan MAT 253 at the University of Maryland, College Park. The analytical uncertainties based on reproducibility of IAEA reference materials in terms of δ^nS values are 0.15, 0.26, and 0.60‰ for n = 33, 34, and 36, respectively (2 s.d.), and in terms of $\Delta^{33}S$ and $\Delta^{36}S$ values are 0.018 and 0.38‰, respectively (2 s.d.). We adopted a rigorous cleaning protocol for the fluorination line prior to our experimental sample fluorinations to avoid any contamination from any residual Ag$_2$S from previous sample fluorinations. Prior to any loading of Ag$_2$S samples from sulfide oxidation experiments, the nickel bombs were emptied of all previous residual aluminum foil packets, reattached and baked for 12–24 h under vacuum (to remove most of the trace adsorbed H$_2$O), and then blank fluorinated overnight 2–3 times.

2.4. Isotope enrichment factors

The isotope enrichment factors ($^n\varepsilon_{P\text{-}R}$) associated with sulfide oxidation are determined by measuring the isotopic composition of the residual reactant sulfide as a function of reaction progress in a closed system following the Rayleigh equation:

$$\ln\left(\frac{^nR_R}{^nR_{R_0}}\right) = {}^n\varepsilon_{P-R} \times \ln(f_R) \tag{4}$$

where ^nR refers to a sulfur isotope ratio ($^nR = {}^nS/^{32}S$; n = 33, 34, or 36), subscript R refers to residual reactant (0 refers to initial), $^n\varepsilon_{P\text{-}R}$ is the isotope enrichment factor (in terms of products, P, relative to reactants, R), f_R is the fraction of reactant remaining (i.e., $[(H_2S)_T]/[(H_2S)_T]_0$), and the trace abundance approximation has been applied (i.e., $f_R = ({}^{32}S_R + {}^{33}S_R + {}^{34}S_R + {}^{36}S_R)/({}^{32}S_{R\_0} + {}^{33}S_{R\_0} + {}^{34}S_{R\_0} + {}^{36}S_{R\_0}) \approx {}^{32}S_R/{}^{32}S_{R\_0}$; Mariotti et al., 1981). This approach has been derived and reviewed in detail elsewhere (e.g., Bigeleisen and Wolfsberg, 1958; Mariotti et al., 1981; Scott et al., 2004), and implemented in previous sulfide oxidation experiments in Fry et al. (1988). This approach assumes only one isotope effect is responsible for the observed isotope fractionation, and that the isotope effect is constant throughout the reaction progress.

Isotope enrichment factors ($^n\varepsilon_{P\text{-}R}$) are related to isotope fractionation factors ($^n\alpha_{P\text{-}R} = {}^nR_P/{}^nR_R$) by Mariotti et al. (1981):

$$^n\varepsilon_{P-R} = {}^{34}\alpha_{P-R} - 1 \tag{5}$$

Enrichment factors ($^n\varepsilon_{P\text{-}R}$) are reported in units of permil (‰).

2.5. Mass dependence of sulfide oxidation

Mass dependent relationships among fractionation factors involving three isotopes are defined as exponential relationships (*cf.* Craig, 1957; Matsuhisa et al., 1978; Clayton and Mayeda, 1996; Miller, 2002), such as:

$$^{33}\alpha_{P-R} = \left(^{34}\alpha_{P-R}\right)^{33/34\theta} \tag{6}$$

$$^{36}\alpha_{P-R} = \left(^{34}\alpha_{P-R}\right)^{36/34\theta} \tag{7}$$

where the $^{33/34}\theta$ and $^{36/34}\theta$ values are the exponents relating mass dependence, and by convention apply strictly to intrinsic fractionation factor relationships between two compounds. The exponential definitions of the $\Delta^{33}S_{P-R}$ and $\Delta^{36}S_{P-R}$ values follow directly from these relationships as deviations from a reference exponent:

$$\Delta^{33}S_{P-R} = {}^{33}\alpha_{P-R} - \left(^{34}\alpha_{P-R}\right)^{0.515} \tag{8}$$

$$\Delta^{36}S_{P-R} = {}^{36}\alpha_{P-R} - \left(^{34}\alpha_{P-R}\right)^{1.9} \tag{9}$$

The reference values of 0.515 and 1.9 are chosen by convention in the definitions of these values to approximate the mass-dependence of most common equilibrium isotope exchange reactions at low temperature (well below the high temperature limit; i.e., $^{33/34}\theta_{equilibrium} \approx 0.515$ and $^{36/34}\theta_{equilibrium} \approx 1.9$).

Exponents of mass dependence associated with sulfide oxidation in this study are computed from experimental data *via* the mathematically equivalent relations to Eqs. (6) and (7):

$$^{33/34}\theta = \frac{\ln\left(^{33}\alpha_{P-R}\right)}{\ln\left(^{34}\alpha_{P-R}\right)} \tag{10}$$

$$^{36/34}\theta = \frac{\ln\left(^{36}\alpha_{P-R}\right)}{\ln\left(^{34}\alpha_{P-R}\right)} \tag{11}$$

The uncertainty associated with the experimentally derived exponents can be straightforwardly estimated solely from the isotopic data collected throughout an experiment *via* the least squares linear regression of $\ln(^{n}R_{R,t}/^{n}R_{R,t=0})$ *vs.* $\ln(^{34}R_{R,t}/^{34}R_{R,t=0})$ (where n = 33 or 36) that computes the exponent associated with a Rayleigh process as $(^{n}\alpha_{P-R}-1)/(^{34}\alpha_{P-R}-1)$, where n = 33 or 36, i.e.:

$$\ln\left(\frac{^{n}R_{R,t}}{^{n}R_{R,t=0}}\right) = \left(\frac{^{n}\alpha_{P-R}-1}{^{34}\alpha_{P-R}-1}\right) \times \ln\left(\frac{^{34}R_{R,t}}{^{34}R_{R,t=0}}\right) \tag{12}$$

We make the assumption that the uncertainty estimate for the value of $(^{n}\alpha_{P-R}-1)/(^{34}\alpha_{P-R}-1)$ from the least squares linear regression is comparable to the uncertainty of the exponent that applies to the fractionation factors $(^{n/34}\theta)$.

3. RESULTS

3.1. Concentration profiles at 25 °C

Plotted in Fig. 1 are representative sulfide concentration profiles of experiments performed at 25 °C as a function of time in terms of fraction of sulfide remaining (i.e., $f = [HS^-]/[HS^-]_{initial}$, brackets denote concentrations) for experiments with and without an added ferrous iron catalyst. The data points are the measured concentrations and the smooth curves are modeled based on a pseudo first order rate law (Section 3.2; Table 2). Many experiments appear to exhibit an induction period where sulfide concentrations do not change appreciably (within the uncertainty of the measurements) that ranges between ~8 and 13 h
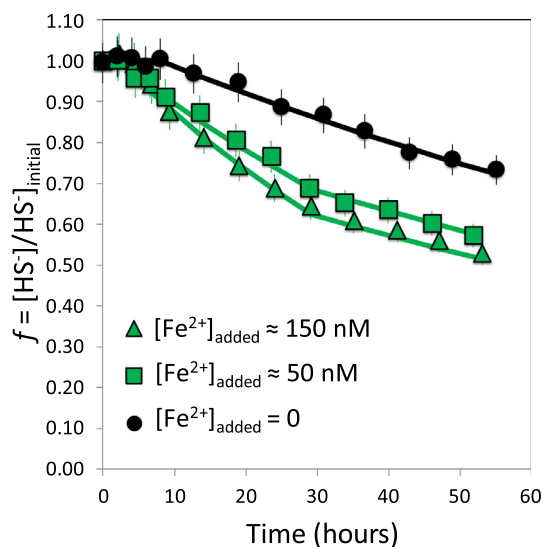

Fig. 1. Representative concentration profiles plotted in terms of fraction of sulfide remaining for oxidation experiments performed at 25 °C (monitored continuously for ~50–55 h), with and without an added ferrous iron catalyst. Uncertainties for individual concentration analyses were typically ≤5% based on either duplicate or triplicate analyses (2 s.d.) (a uniform 5% uncertainty is plotted for reference). The solid curves represent pseudo first-order kinetic models based on fits to experimental sulfide concentration data.

for the experiments where no ferrous iron was added to a few hours for experiments where ferrous iron was added (Table 2). A pronounced induction period of 36–48 h was also observed in the experiments where no ferrous iron was added performed at 5 °C (Table 2; see also Supplementary Materials). The precision of the duration of the induction period is limited by the chosen sampling interval. For the extraction of the pseudo first order rate constants, concentrations during the induction period are not taken into consideration where applicable. The two sets of explicitly catalyzed experiments where ferrous iron was added exhibit a distinct break in rate near the 30-hour mark. For these experiments, two individual pseudo first order rate constants were extracted from the experimental data: one prior to the break in rate (denoted "Before Break"), and one following the break in rate (denoted "After Break") (Table 2).

Similar plots showing reaction products measured (i.e., SO_3^{2-}, $S_2O_3^{2-}$) are provided in the Supplementary Material. We observe a lag in the in-growth of products that is consistent with the lag in the disappearance of sulfide (see Supplementary Material). The measured concentrations of sulfite and thiosulfate are relatively low (≤20–30 μM) over the duration of our experiments and are consistent with the relatively low extents of reaction studied. The remaining sulfur that was not analyzed (presumed to be mostly SO_4^{2-}; *cf.* Zhang and Millero, 1993a) is similarly relatively low in concentration (≤20–40 μM). The low concentrations of these products in each of our experiments precluded their isotopic analysis, which is why we focus only on the isotopic analyses of sulfide in this study.

Table 2
Experimental conditions and rate parameters from sulfide oxidation experiments. The reported pH values are averages of measurements performed on 5–6 aliquots taken throughout experimental runs. Subscripts on concentration values indicate: T = total dissolved species in solution (e.g., $[(CO_3^{2-})_T] = [CO_3^{2-}] + [HCO_3^-]$), i = initial concentrations (*italics* indicate estimated values), and added = amount added. I.P. is the estimated induction period (N/A = not clearly resolved). k' is the pseudo first order rate constant (Eq. (3)) and k is the computed second order (overall) rate constant using the estimated $[O_2]_i$ and assuming b = 1 (*cf.* Table 1). The two sets of rate constants derived from the ferrous iron catalyzed experiments indicate values before the pronounced break in rate ("Before Break") and after ("After Break") (see Fig. 1). Uncertainties are 2 s.d.

Identifier	T (°C)	pH	$[(CO_3^{2-})_T]$ (M)	$[(H_2S)_T]_i$ (µM)	$[O_2]_i$ (µM)[‡]	$[Fe^{2+}]_{added}$ (nM)	I.P. (h)	k' (h^{-1})	k (M^{-1} hr^{-1})	ln$k$	k' (hr^{-1})	k (M^{-1} hr^{-1})	ln$k$
SOX-5[*]	5	9.77 ± 0.15	0.002	224	*399*	0	~36–48	0.0021 ± 0.0002	5.15 ± 0.42	1.64 ± 0.08			
SOX-25(A)[*]	25	9.80 ± 0.02	0.02	226	*258*	0	~6–8	0.0109 ± 0.0016	42.4 ± 6.1	3.75 ± 0.14			
SOX-25(B)[*]	25	9.78 ± 0.09	0.02	214	*258*	0	N/A	0.0084 ± 0.0013	32.4 ± 5.0	3.48 ± 0.15			
SOX-25(C)	25	9.91 ± 0.09	0.002	226	*258*	0	~8–13	0.0069 ± 0.0005	26.8 ± 2.0	3.29 ± 0.07			
SOX-25(D)	25	9.73 ± 0.09	0.002	227	*258*	0	~8–13	0.0082 ± 0.0008	31.6 ± 3.2	3.45 ± 0.10			
Average (SOX-25)		***9.81 ± 0.08***						***0.0086 ± 0.0034***	***33.3 ± 13.2***	***3.49 ± 0.38***			
SOX-45[*]	45	9.94 ± 0.05	0.002	221	*186*	0	N/A	0.0243 ± 0.0025	131 ± 13	4.87 ± 0.10			
Experiments with ferrous iron added								"Before Break"			"After Break"		
SOX-Fe50(A)[*]	25	9.82 ± 0.02	0.02	220	*258*	46	~6–8	0.0153 ± 0.0016	59.1 ± 6.4	4.08 ± 0.11	0.0077 ± 0.0016	29.8 ± 6.1	3.39 ± 0.21
SOX-Fe50(B)[*]	25	9.78 ± 0.09	0.02	225	*258*	46	~4–6	0.0139 ± 0.0015	53.9 ± 5.6	3.99 ± 0.10	0.0077 ± 0.0009	29.8 ± 3.6	3.39 ± 0.12
Average (SOX-Fe50)		***9.80 ± 0.04***						***0.0146 ± 0.0019***	***56.5 ± 7.4***	***4.03 ± 0.13***			
SOX-Fe150[*]	25	9.81 ± 0.05	0.02	226	*258*	153	~2	0.0175 ± 0.0013	67.9 ± 5.0	4.22 ± 0.07	0.0081 ± 0.0007	31.3 ± 2.9	3.44 ± 0.09

Bold italic indicates that these are average values (± standard deviation) for the quantities of chosen condition.

[‡] Estimated under experimental conditions after Benson and Krause (1980; 1984) (http://water.usgs.gov/software/DOTABLES/).

[*] Indicates experiments where isotope data were collected for estimation of fractionation factors (*cf.* Table 3).

3.2. Rate constants

The computed second order rate constants derived from our experiments (Table 2) are plotted in Fig. 2 as a function of inverse temperature in a classic Arrhenius plot. Rate constants from the comparable experiments of Millero et al. (1987) and Luther et al. (2011) are shown for reference and discussion (Section 4.1). Our calculated second order rate constants might be viewed as minimum values due to the assumption that our experimental solutions were in equilibrium with ambient air at the experimental temperatures. The least squares linear regression of the data in Fig. 2 (experiments without added ferrous iron catalyst) yields an apparent activation energy of $E_a = 60 \pm 5$ kJ/mol following the Arrhenius equation ($\ln k = -E_a/RT + \ln(A)$; R = ideal gas constant, T = temperature in K, and A is the 'pre-exponential' factor). The second order rate constants from the explicitly catalyzed ferrous iron experiments (denoted "Before Break" in Table 2) are a factor of ∼1.5–2 times higher than those where no ferrous iron was added. The second order rate constants from ferrous iron catalyzed experiments following the pronounced break in rate (denoted "After Break" in Table 2) are indistinguishable from those extracted from experiments without added ferrous iron.
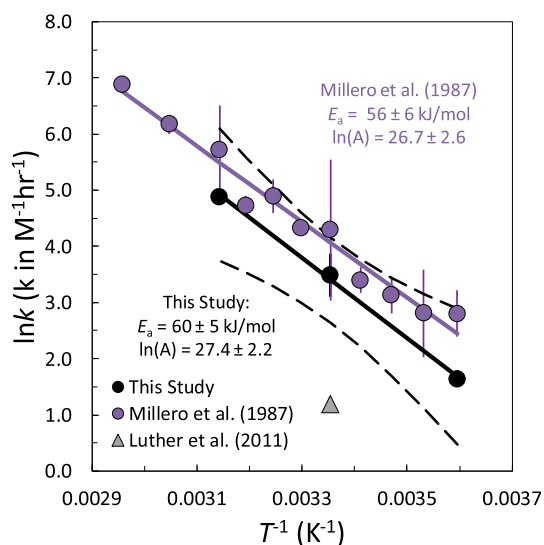

Fig. 2. Overall second order rate constants calculated from our experimental data (black circles) plotted as a function of inverse temperature in a classic Arrhenius plot. The apparent activation energy (E_a) is derived from the slope of the relationship (black line) following the Arrhenius equation ($\ln k = -E_a/RT + \ln(A)$; R = ideal gas constant, T is temperature, and A is the pre-exponential factor), and is based on a least squares linear regression (95% confidence intervals are plotted as dashed black curves). Also plotted for reference are data from Millero et al. (1987) (purple circles) and Luther et al. (2011) (grey triangle). (For interpretation of the references to colour in this figure legend, the reader is referred to the web version of this article.)

3.3. Isotopic compositions of sulfide and isotope enrichment factors

Table 3 summarizes the isotopic composition of sulfide (relative to the initial composition of sulfide in a given experiment) as a function of sulfide remaining in our oxidation experiments. For all experiments, the isotopic composition of sulfide increases in magnitude as a function of reaction progress, which is indicative of a 'normal' isotope effect where products are isotopically depleted relative to reactants. The isotopic composition of residual sulfide changes by only ∼2.4 to 3.7‰ based on $^{34}S/^{32}S$ over the entirety of experimental runs for all experiments, which span a range of reaction completion ($1 - f_{\text{sulfide}}$) of ca. 33–47% based on sulfide.

Fig. 3 illustrates how isotope enrichment factors are determined by the least squares linear regressions for all three sulfur isotope ratios as a function of reaction progress via the Rayleigh equation (Eq. (4)). Table 3 contains a summary of the isotope enrichment factors derived this way from all experiments. The strong linear correlation between the plotted variables based on the strong correlation coefficients (e.g., $r^2 = 0.979$–0.999 for $^{34}\varepsilon_{\text{P-R}}$) and low p-values ($p \leq 0.03$) supports the hypothesis that only one isotope effect is responsible for the observed fractionations. We would expect deviations from these linear relationships that are not apparent in our data if different and competing isotope effects were in operation during different extents of reaction or if full reversibility extending all the way from reactants to products were taking place.

Isotope enrichment factors derived from experiments under all conditions are similar in magnitude and may vary only subtly as a function of the overall rate constant over the ranges we have studied. Major isotope enrichment factors ($^{34}\varepsilon_{\text{P-R}}$) obtained from experiments performed at different temperatures without added ferrous iron are: $^{34}\varepsilon_{\text{P-R}} = -5.05 \pm 0.25$‰ at 5 °C (2 s.d., 1 experiment), -5.85 ± 0.31‰ at 25 °C (2 s.d., 2 experiments), and -6.34 ± 0.49‰ at 45 °C (2 s.d., 1 experiment) (Table 3). Enrichment factors ($^{34}\varepsilon_{\text{P-R}}$) obtained from experiments at 25 °C where trace levels of ferrous iron were added are: $^{34}\varepsilon_{\text{P-R}} = -5.63 \pm 0.65$‰ for $[Fe^{2+}]_{\text{added}} \sim 50$ nM (2 s.d., 2 experiments), and -4.90 ± 0.23‰ for $[Fe^{2+}]_{\text{added}} \sim 150$ nM (2 s.d., 1 experiment) (Table 3). Major isotope enrichment factors ($^{34}\varepsilon_{\text{P-R}}$) might exhibit very slight relationships with increasing overall rate constant due to both changes in temperature and the addition of the ferrous iron catalyst at trace levels (Fig. 4a). Enrichment factors ($^{34}\varepsilon_{\text{P-R}}$) might decrease in magnitude with increasing rate due to ferrous iron catalysis, and might increase in magnitude with increasing rate due to increasing temperature. However, these variations are relatively small and are very near the estimated uncertainty of the measurements. Fig. 4(b) is a plot of the enrichment factors as a function of inverse temperature for experiments where no ferrous iron was added, which additionally include computed 95% confidence intervals where it is noted that the estimated temperature dependence of the enrichment factor is relatively weak over the range we have investigated. We have not attempted to

Table 3
Isotopic analyses of sulfide from oxidation experiments. Definition of terms: $f = [HS^-]/[HS^-]_{initial}$, $\delta^n S' = 1000 \times \ln(^n R/^n R_{initial})$ (units of ‰; where n = 33, 34, 36 and $^n R = {}^n S/{}^{32}S$). Fractionation factors are computed via the Rayleigh equation (Eq. (4)) and are reported as: $^n \varepsilon_{P-R} = (^n \alpha_{P-R} - 1) \times 1000$, P = products, R = reactant (units of ‰). The uncertainties (2 s.d.) and other italicized data (r^2 correlation coefficients and p-values) are based on least square linear regressions. For reference, estimated uncertainties on $\delta^n S'$ based on long-term reproducibility of reference standards are 0.15, 0.26, and 0.60‰ for n = 33, 34, and 36, respectively (2 s.d.).

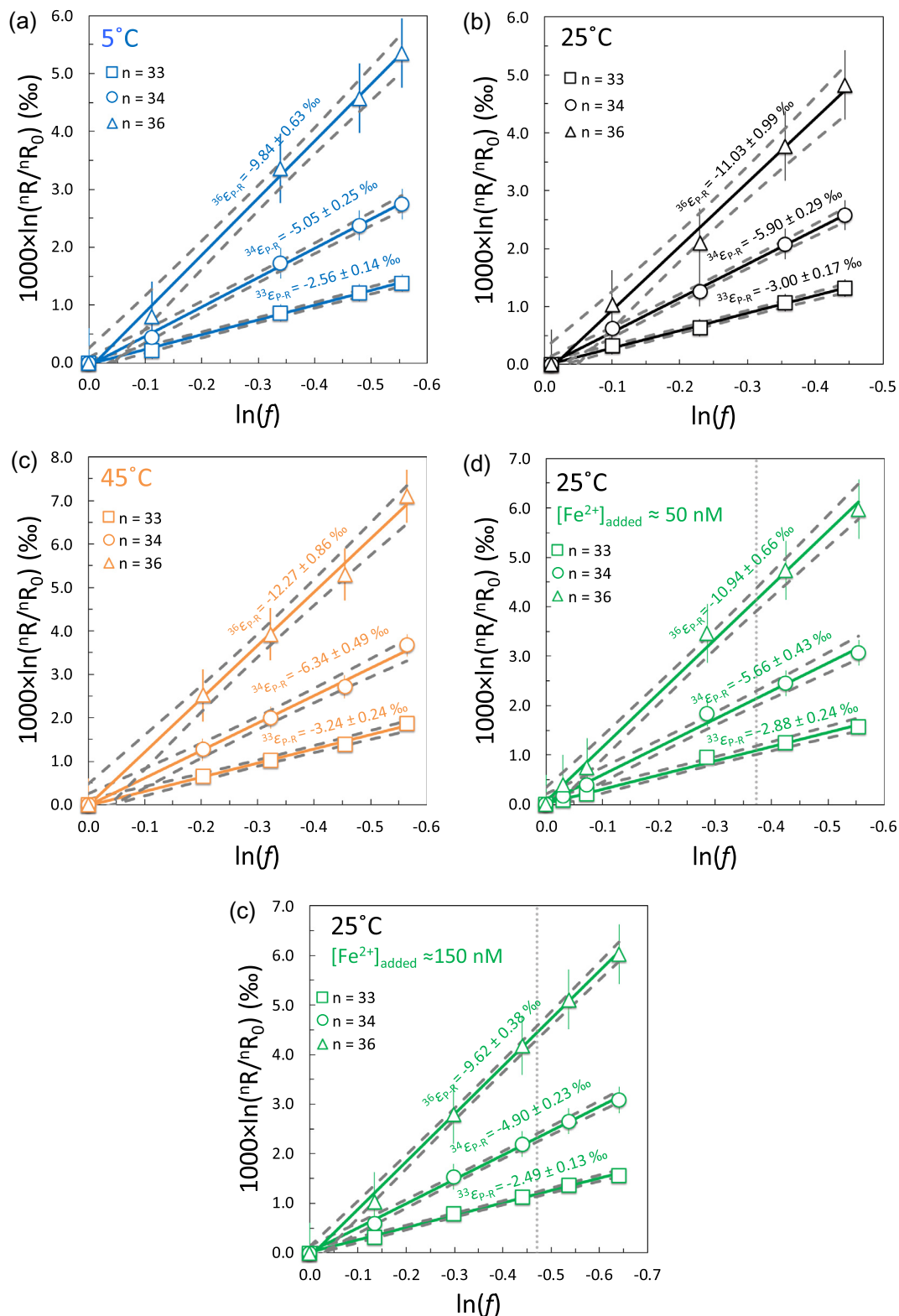| Identifier	T (°C)	$[Fe^{2+}]_{added}$ (nM)	f	$\delta^{33}S'$	$\delta^{34}S'$	$\delta^{36}S'$		$^{33}\varepsilon_{P-R}$	$^{34}\varepsilon_{P-R}$	$^{36}\varepsilon_{P-R}$	$^{33/34}\theta$	$^{36/34}\theta$	$\Delta^{33}S_{P-R}$	$\Delta^{36}S_{P-R}$
SOX-5	5	0	1.00	0.00	0.00	0.00		−2.56	−5.05	−9.84	0.507	1.95	0.039	−0.27
			0.89	0.22	0.45	0.80	2 s.d.	0.14	0.25	0.63	0.006	0.04	0.032	0.19
			0.71	0.86	1.73	3.36	r^2	0.998	0.998	0.997	0.999	0.999		
			0.62	1.21	2.38	4.57	p	0.01	0.01	0.02				
			0.57	1.39	2.75	5.35								
SOX-25(A)	25	0	0.99	0.00	0.00	0.00		−3.00	−5.90	−11.03	0.509	1.88	0.036	0.14
			0.90	0.32	0.62	1.03	2 s.d.	0.17	0.29	0.99	0.005	0.12	0.032	0.71
			0.79	0.64	1.26	2.09	r^2	0.998	0.998	0.994	0.999	0.997		
			0.70	1.06	2.08	3.77	p	0.01	0.01	0.02				
			0.64	1.32	2.58	4.82								
SOX-25(B)	25	0	1.00	0.00	0.00	0.00		−2.96	−5.81	−11.38	0.510	1.96	0.030	−0.37
			0.98	0.03	0.07	0.23	2 s.d.	0.27	0.54	0.97	0.003	0.04	0.019	0.21
			0.83	0.61	1.21	2.39	r^2	0.994	0.994	0.995	1.000	0.999		
			0.72	0.90	1.78	3.53	p	0.02	0.03	0.03				
			0.67	1.21	2.38	4.71								
SOX-45	45	0	1.00	0.00	0.00	0.00		−3.24	−6.34	−12.27	0.510	1.94	0.030	−0.25
			0.82	0.64	1.27	2.52	2 s.d.	0.24	0.49	0.86	0.003	0.02	0.019	0.15
			0.72	1.02	2.00	3.92	r^2	0.996	0.996	0.996	1.000	0.999		
			0.64	1.39	2.71	5.29	p	0.00	0.01	0.01				
			0.57	1.87	3.67	7.10								
SOX-25-Fe50(A)	25	~50	1.00	0.00	0.00	0.00		−2.88	−5.66	−10.94	0.508	1.94	0.039	−0.21
			0.97	0.09	0.18	0.40	2 s.d.	0.24	0.43	0.66	0.006	0.04	0.031	0.22
			0.93	0.21	0.40	0.74	r^2	0.993	0.994	0.996	0.999	0.999		
			0.75	0.95	1.83	3.46	p	0.01	0.02	0.02				
			0.65	1.25	2.45	4.73								
			0.57	1.56	3.07	5.97								
SOX-25-Fe50(B)	25	~50	1.00	0.00	0.00	0.00		−2.83	−5.59	−10.77	0.506	1.93	0.051	−0.17
			0.96	0.04	0.11	0.37	2 s.d.	0.43	0.83	1.54	0.005	0.09	0.028	0.48
			0.91	0.17	0.36	1.02	r^2	0.978	0.979	0.980	0.9999	0.998		
			0.77	0.92	1.83	3.65	p	0.01	0.02	0.02				
			0.65	1.17	2.32	4.67								
			0.57	1.50	2.98	5.82								
SOX-25-Fe150	25	~150	1.00	0.00	0.00	0.00		−2.49	−4.90	−9.62	0.507	1.97	0.037	−0.33
			0.87	0.32	0.60	1.03	2 s.d.	0.13	0.23	0.38	0.006	0.07	0.031	0.34
			0.74	0.79	1.54	2.80	r^2	0.998	0.998	0.998	0.999	0.999		
			0.64	1.13	2.20	4.19	p	0.00	0.00	0.00				
			0.58	1.37	2.66	5.11								
			0.53	1.56	3.08	6.03								

Fig. 3. Plots illustrating how isotope enrichment factors ($^n\varepsilon_{P-R} = {}^n\alpha_{P-R} - 1$, P = products, R = reactant) are derived from experimental data *via* the Rayleigh equation (Eq. (4)) in this study, where $^nR = {}^nS/{}^{32}S$ (n = 33, 34, 36) and refer to the isotopic composition of residual sulfide relative to its initial composition ($^nR_0$). (a)–(c) correspond to experiments where no catalyst was added, and were conducted at 5 °C (a), 25 °C (b), and 45 °C (c); and (d)-(e) correspond to experiments performed with added amounts of trace ferrous iron performed at 25 °C: (d) $[Fe^{2+}]_{added} \sim 50$ nM, and (e) $[Fe^{2+}]_{added} \sim 150$ nM. The vertical gray dotted lines in (d)–(e) indicate the break in rate observed in these experiments (*cf.* Fig. 1). Uncertainties on isotope enrichment factors are 2 s.d. and are based on the least squares linear regressions (see also Table 3). Grey dotted curves correspond to the calculated 95% confidence intervals for each linear regression. The error bars on individual analyses are estimates (2 s.d.) based on the long-term reproducibility of IAEA reference standards.
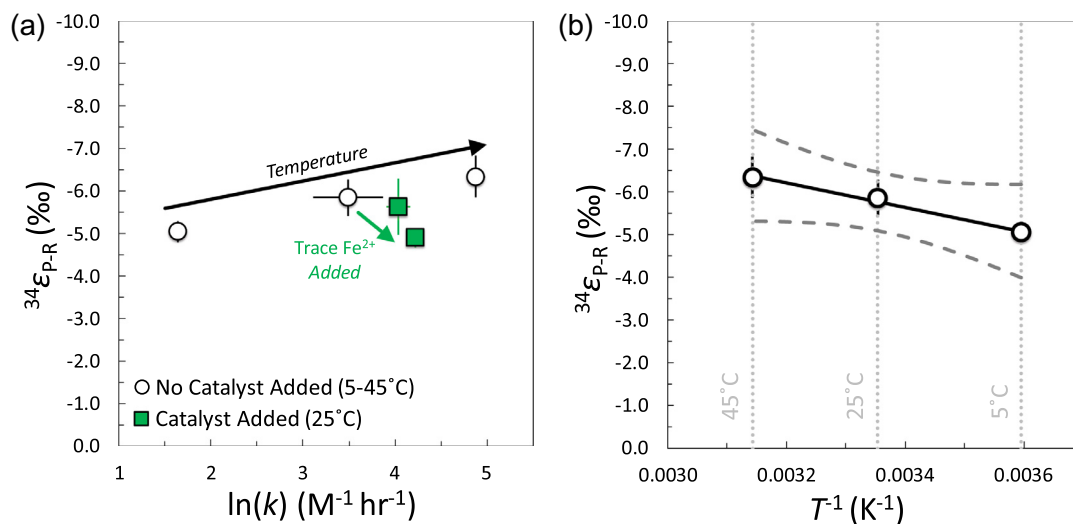
Fig. 4. Major isotope enrichment factors ($^{34}\varepsilon_{P\text{-}R}$) derived from our experiments and plotted as a function of (a) computed overall second order rate constant for all experimental conditions (arrows indicate direction of increasing temperature and ferrous iron added), and (b) inverse temperature (in units of K^{-1}) for the experiments performed without an added trace metal catalyst, where the grey curves are computed 95% confidence intervals. Error bars correspond to 2 s.d. based on linear regressions and experimental reproducibility (latter where applicable; see Tables 2 and 3).

quantify a temperature dependence for values of $^{34}\varepsilon_{P\text{-}R}$ from this relationship.

Quantities related to the mass dependence of fractionations ($\Delta^{33}S_{P\text{-}R}$, $\Delta^{36}S_{P\text{-}R}$, $^{33/34}\theta$ and $^{36/34}\theta$) are illustrated in Fig. 5. The exponents associated with equilibrium isotope exchange among aqueous sulfur compounds derived from theoretical calculations are plotted for reference (Eldridge et al., 2016). The measured $^{33/34}\theta$ appear to be lower in magnitude than exponents expected from equilibrium isotope exchange (Fig. 5a), which is additionally exhibited in slightly positive $\Delta^{33}S_{P\text{-}R}$ values (Fig. 5b). Any relationships between $^{33/34}\theta$ and $\Delta^{33}S_{P\text{-}R}$ with rate as functions of both ferrous iron catalysis and temperature are not resolved over the range we have studied (e.g., Fig. 5b). The measured values for $^{36/34}\theta$ and $\Delta^{36}S_{P\text{-}R}$ may also exhibit deviations from equilibrium isotope exchange but are not resolved under all experimental conditions and, similarly, do not appear to exhibit any resolvable relationships with reaction rate due to explicit ferrous iron catalysis or temperature (Fig. 5c and d). For reference, the computation of mean values for all reported experiments yield: $^{33/34}\theta = 0.508 \pm 0.003$, $\Delta^{33}S_{P\text{-}R} = 0.037 \pm 0.014‰$, $^{36/34}\theta = 1.94 \pm 0.06$, and $\Delta^{36}S_{P\text{-}R} = -0.21 \pm 0.34‰$ (2 s.d., 7 experiments based on 38 isotopic analyses; from Table 3).

4. DISCUSSION

4.1. Rate constants and Arrhenius parameters: Comparison to previous experiments

Second order rate constants derived from previous experiments performed in low ionic strength buffer solutions (Avrahami and Golding, 1968; O'Brien and Birkner, 1977; Millero et al., 1987; Zhang and Millero, 1993a; Luther et al., 2011) are plotted in Fig. 6a as a function of

pH along with our own for comparison. We focus primarily on experiments performed at high pH where HS^- dominates the speciation that are comparable to our experiments (the pK_a for $H_2S = HS^- + H^+$ at 25 °C is additionally plotted in Fig. 6a for $\mu = 0$ and 0.1 m from Hershey et al., 1988). From experiments performed at 55 °C, Millero et al. (1987) found that the rates of sulfide oxidation as a function of pH largely reflect the speciation of sulfide, where the second order rate constant appears to have a near constant value under pH conditions where either HS^- or H_2S individually dominate the speciation (where $k_{H2S} < k_{HS^-}$), and intermediary values under circumneutral pH conditions where both are present in appreciable amounts. Similar experiments of Zhang and Millero (1993a) performed at 45 °C in similarly low ionic strength solutions show similar relationships with pH. For illustrative context, we plot the experiments of Millero et al. (1987) and Zhang and Millero (1993a) as a function of pH originally performed at 55 °C or 45 °C and corrected for temperature using their 25 °C determinations and roughly corrected for any pH shifts that may occur due to temperature using the dissociation quotients of Hershey et al. (1988). The experimental determinations in Fig. 6a (including this study) define a range in the second order rate constant that spans well over an order of magnitude under pH conditions above 8, far outside the range of what might be expected from the broad observations of pH dependence from Millero et al. (1987) and Zhang and Millero (1993a).

Luther et al. (2011) report the lowest second order rate constant observed to date from experiments performed under trace metal clean conditions. The experiments of Luther et al. (2011) were performed in Mg^{2+}-scrubbed NaOH (25 °C, pH ∼ 12) in a class 100 clean bench utilizing triple acid-washed plastic reaction tubes (cleaned in trace metal clean HCl), and yield an overall rate constant that
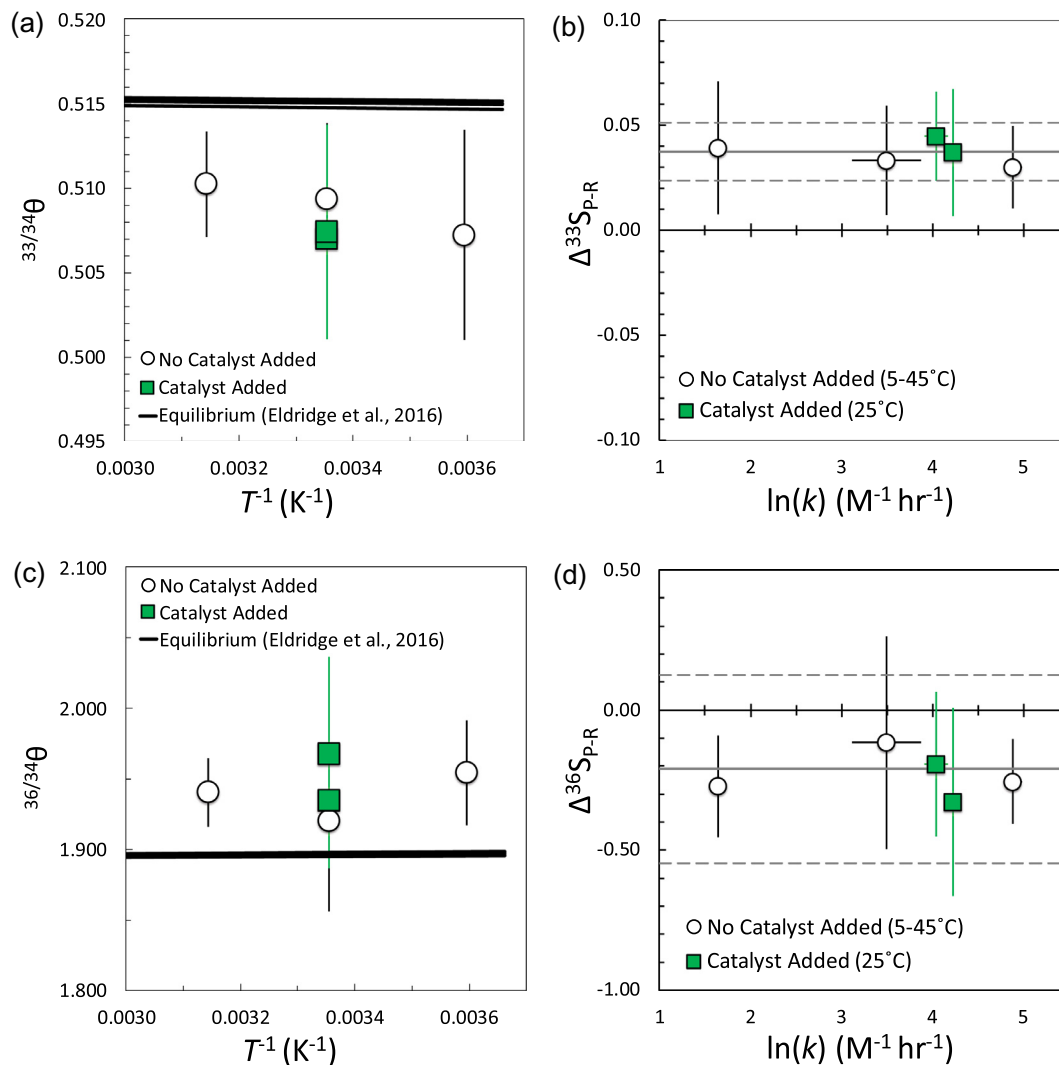
Fig. 5. Quantities relating to the mass-dependence of fractionations associated with sulfide autoxidation: (a) $^{33/34}\theta$-values derived from all experimental conditions plotted as a function of inverse temperature (K^{-1}), where $^{33/34}\theta_{equilibrium}$ associated with numerous equilibrium isotope exchange reactions among aqueous sulfur compounds involving HS^{-} (black curves) are shown for reference (HS^{-}/S*-SO$_3^{2-}$, HS^{-}/SO$_2^{2-}$, HS^{-}/SO$_3^{2-}$, and HS^{-}/SO$_4^{2-}$; from Eldridge et al., 2016); (b) $\Delta^{33}S_{P-R}$ (in units of ‰) derived from experiments plotted as a function of the overall second order rate constant for all conditions studied, where the grey lines represent the mean (solid) and 2 s.d. of the mean (dashed) for all conditions; and (c) and (d) contain the analogous plots for values of $^{36/34}\theta$ and $\Delta^{36}S_{P-R}$ (in units of ‰), respectively. All error bars are 2 s.d.

is ca. 10x lower than those of Millero et al. (1987) (on average) and ca. 5x lower than our experiments (Table 1, Figs. 2 and 6). Assuming that the broad observations regarding the pH dependence of the reaction rate are valid at 25 °C (Millero et al., 1987; Zhang and Millero, 1993a) and the reaction remains second order overall (a = 1, b = 1), the data of Luther et al. (2011) may suggest that much of the variability seen in Fig. 6a at high pH is due to varying levels of unintended trace metal catalysts impacting the experimental determination of rates. Trace metal catalysts are documented to cause several order of magnitude changes in the apparent overall second order rate constants associated with sulfide oxidation under otherwise equivalent conditions even at relatively low (nM) levels depending

on the metal (Vazquez et al., 1989). Trace metal (or perhaps other catalytic) contaminants in the reagents (e.g., buffer salts), the reaction vessel and its components, and/or atmosphere in the laboratory environment appear to be among the likely causes but are ultimately unknown.

A direct comparison to the experimental dataset of Chen and Morris (1972a) is more difficult due to the different rate law parameters derived from their experimental data than most other studies (i.e., a = 1.34 and b = 0.56 with a rate constant in units of M$^{-0.9}$ hr^{-1}; Table 1). Chen and Morris (1972a) also observed apparent patterns in the rate of oxidation at 25 °C as a function of pH (6–12.5) where maximum rates were found at a pH of ~8 and ~11 with a local minimum at a pH of ~9 (difference between
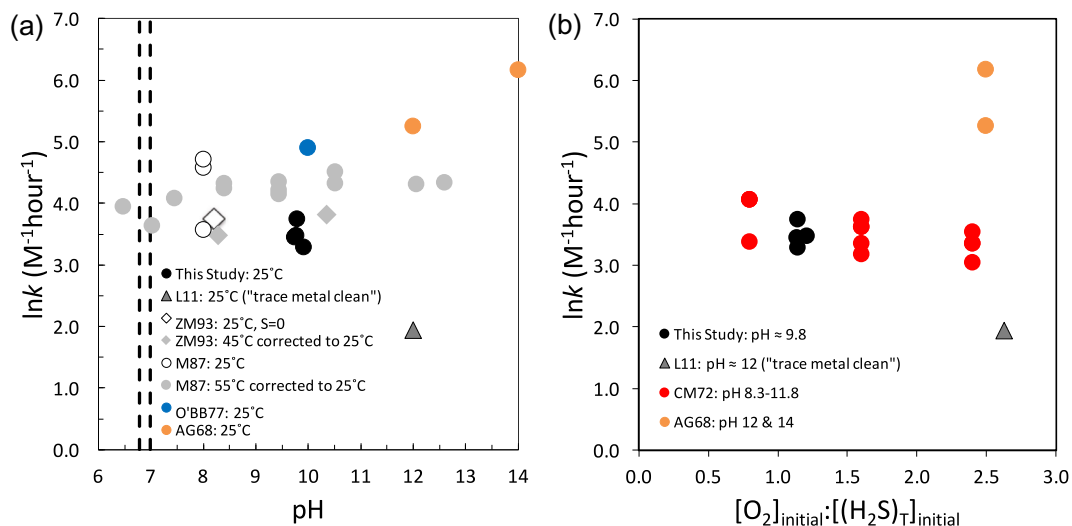
Fig. 6. Compilation of second order rate constants (k) derived from this study and the literature: (a) Second order rate constants derived from experiments in low ionic strength buffer solutions (i.e., not seawater) as a function of pH. The vertical dashed lines indicate the range of the first dissociation constant for H_2S ($pK = -\log K$) over ionic strength of $\mu = 0–0.1$ m from Hershey et al. (1988). (b) Computed second order rate constants derived from the rate data of Chen and Morris (1972a) from experiments comparable to the present study as a function of the initial molar oxygen to sulfide ratio, with a handful of other experimental studies shown for reference. References: AG68 = Avrahami and Golding (1968), CM72 = Chen and Morris (1972a), O'BB77 = O'Brien and Birkner (1977), M87 = Millero et al. (1987), ZM93 = Zhang and Millero (1993a), and L11 = Luther et al. (2011).

max/min is on the order of a factor of three), which were not reproduced by Millero et al. (1987) at 55 °C (Fig. 6a). To make rough comparisons to our experiments, we focus on experiments from Chen and Morris (1972a) performed under the most comparable conditions to our own: $[H_2S_T]_{initial} = 200\ \mu M$ under relatively low initial $[O_2]_{initial}$: $[(H_2S)_T]_{initial}$ ratios (i.e., $[O_2]_{initial} = 160–480\ \mu M$) over $pH = 8.34–11.75$. We use their reported data to re-derive the initial rates of sulfide oxidation determined from their experiments and then assume a = 1 and b = 1 and the given initial sulfide and oxygen concentrations to compute a hypothetical second order rate constant to put on more comparative grounds to our own. These are plotted in Fig. 6b as a function of the $[O_2]_{initial}$:$[(H_2S)_T]_{initial}$ ratio of the experiment (along with other experiments performed under comparable $[O_2]_{initial}$:$[(H_2S)_T]_{initial}$; Avrahami and Golding, 1968; Luther et al., 2011). Computed this way, our rate constants are similar to the Chen and Morris (1972a) experiments, where the second order rate constants computed from our repeat experiments span a similar range as those computed from Chen and Morris (1972a) as a function of pH under otherwise similar conditions.

The activation energy that we derive from our experiments (60 ± 5 kJ/mol: Fig. 2) is indistinguishable from Millero et al. (1987) (56 ± 6 kJ/mol) (0.02 M borate buffer, $pH = 8.0$, T = 5–65 °C) despite our computed overall rate constants being on the lower end of their range. From an examination of the 95% confidence intervals for our data in Fig. 2, the apparent offset may be reasonably assumed to be within the error of the determinations. It is possible that our estimates of the second order rate constants are biased slightly low due to the assumption that our experiments were saturated with respect to oxygen from air. If

this is the case, any bias must be systematic as a function of temperature in order to obtain a similar activation energy to Millero et al. (1987). We took a similar approach to Millero et al. (1987) to saturate our experiments with air and bubbled our buffer solutions with ambient air for 1 h prior to the injection of sulfide.

4.2. Mechanisms of sulfide oxidation

It is generally understood that sulfide autoxidation follows second order kinetics overall (Table 1). A second order rate law (a = 1, b = 1) for sulfide autoxidation requires a mechanism that yields an overall 1:1 sulfide to oxygen consumption stoichiometry. Additionally, any elementary reactions that consume sulfide are likely to involve either one or two electron transfer reactions in order to be feasible. Reactions that appear to fit these criteria include (e.g., Chen and Morris, 1972a,b; Hoffmann and Lim, 1979; Zhang and Millero, 1993a; Luther, 2010):

$$HS^- + O_2 \rightarrow HS^\bullet + O_2^- \tag{13}$$

$$HS^- + O_2 \rightarrow S^0 + HO_2^- \tag{14}$$

When a trace metal is involved (M^{n+}) that was either intentionally added or unintentionally present as part of the experimental background conditions, the following may occur:

$$HS^- + M^{n+} \rightarrow HS^\bullet + M^{(n-1)+} \tag{15}$$

$$M^{(n-1)+} + O_2 \rightarrow M^{n+} + O_2^- \tag{16}$$

These two steps involving $M^{n+}/M^{(n-1)+}$ yield Eq. (13) as an overall reaction. An alternative possibility for an oxygen-reactive trace metal catalyst begins with the trace

metal undergoing autoxidation. For example, catalysis *via* Fe^{2+} that has been investigated in the present study may involve (e.g., Millero, 1986; Zhang and Millero, 1993a):

$$Fe^{2+} + O_2 \rightarrow Fe^{3+} + O_2^- \tag{17}$$

$$HS^- + Fe^{3+} \rightarrow HS^\bullet + Fe^{2+} \tag{18}$$

Eqs. (17) and (18) also yield Eq. (13) as an overall reaction.

The reaction products of Eq. (13) ($HS^\bullet$ and O_2^-) may be highly reactive towards one another, and may yield:

$$HS^\bullet + O_2^- \rightarrow S^0 + HO_2^- \tag{19}$$

Combining Eq. (13) with Eq. (19) yields Eq. (14), therefore Eq. (14) can be viewed as either an elementary two electron transfer reaction (as written) or as an overall reaction comprised of multiple one electron transfer reactions. In principle, the superoxide (O_2^-) produced by Eqs. (13), (16) and/or (17) can also undergo reaction with residual sulfide:

$$HS^- + O_2^- \rightarrow HS^\bullet + O_2^{2-} \tag{20}$$

The peroxide (HO_2^- or H_2O_2) produced by Eq. (14) (overall or stepwise), (19), and/or (20) may also serve as a strong oxidant for sulfide (e.g., Millero et al., 1989):

$$HS^- + H_2O_2 \rightarrow HS^\bullet + HO^\bullet + OH^- \tag{21}$$

Thus, numerous reaction pathways may be available to sulfide as part of the overall autoxidation process. It would appear that any of the one to two electron transfer reactions between HS^- and an oxygen species (e.g., O_2, O_2^-, HO_2^-/H_2O_2) with or without a trace metal catalyst could represent rate determining step(s) and be consistent with the observed reaction orders.

Two overall reaction mechanisms have been proposed to explain the remainder of the sulfide autoxidation process that largely attempt to link the hypothetical initial products of sulfide consumption (i.e., $HS^\bullet$ and/or S^0) to the intermediates and products (ultimate end product: SO_4^{2-}) that have been detected and/or are observed to accumulate. The observed intermediates that are observed to accumulate principally include sulfite (SO_3^{2-}) and thiosulfate ($S_2O_3^{2-}$) (e.g., Zhang and Millero, 1993a; analyzed in the present study). Far less commonly observed are the polysulfides (S_x^{2-}, x = 2–8; Chen and Morris, 1972a) and possibly sulfoxylate (SO_2^{2-}/HSO_2^-; Vairavamurthy and Zhou, 1995; Tossell, 1997), which is in part due to the chemical assays available for these compounds and their corresponding detection limits, and the potentially high turnover of these highly reactive compounds. The two mechanisms have been described as the polar mechanism (Hoffmann and Lim, 1979) and the free radical chain mechanism (e.g., Chen and Morris, 1972a; Zhang and Millero, 1993a). Schematic representations of the two mechanisms are presented in Fig. 7 for reference (drawn after Zhang and Millero, 1993a). As far as the authors are aware, neither of these mechanisms has been satisfactorily ruled-out or confirmed and the process of autoxidation could draw upon aspects of each. The key point to take away from these hypothetical mechanisms for the purposes of the present study is that
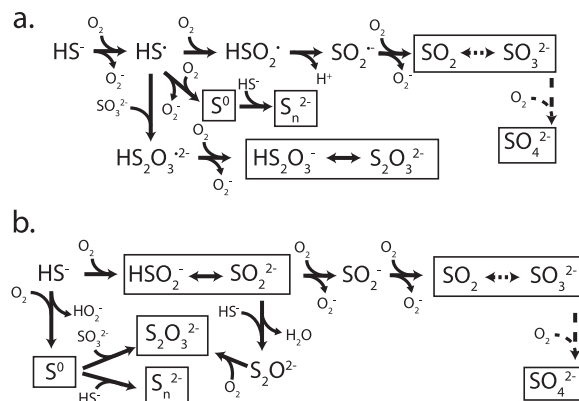

Fig. 7. Schematic representations of the two major mechanisms that have been proposed for sulfide autoxidation (drawn after Zhang and Millero, 1993a). (a) The free radical mechanism (Chen and Morris, 1972a), and (b) the polar mechanism (Hoffmann and Lim, 1979; Zhang and Millero, 1993a). The boxes indicate intermediate or product compounds that have been detected in sulfide oxidation experiments: sulfite (SO_3^{2-}), thiosulfate ($S_2O_3^{2-}$), and sulfate (SO_4^{2-}) are commonly observed (e.g., Zhang and Millero, 1993a); polysulfides (S_n^{2-}) were detected in the circum-neutral pH experiments of Chen and Morris (1972a); and sulfoxylate (SO_2^{2-}) was reported to have been detected *via* XANES spectroscopy by Vairavamurthy and Zhou (1995). Mechanisms for the subsequent oxidation of most intermediates are omitted for simplicity. The dashed arrow representing the oxidation of sulfite to sulfate *via* O_2 represents an overall reaction (non-stoichiometric drawn) that proceeds through a highly complex free radical chain mechanism of its own (Connick et al., 1995; Connick and Zhang, 1996). The oxygen species O_2^- (superoxide) and HO_2^-/O_2^{2-} (peroxide) generated by numerous reactions in each mechanism are referred to as reactive oxygen species (ROS) throughout the text.

many of the downstream reactions involving sulfur intermediates have the potential to generate the reactive oxygen species (O_2^-, HO_2^-) that could serve as autocatalysts for the overall autoxidation of aqueous sulfide, which could explain some of the broad behavior we see in our experiments (e.g., induction periods).

4.3. Induction period

Most of our sulfide oxidation experiments exhibit a resolvable induction period before any obvious reaction proceeds (Table 2; Fig. 1). The duration of the induction period is a function of temperature (e.g., decreases from ~36–48 h at 5 °C to ~8–12 h at 25 °C to undetectable at 45 °C) and possibly the degree of explicit ferrous iron catalysis. The presence of an induction period suggests that the reaction is autocatalytic and requires the build-up of a key intermediate (or intermediates) to effective concentrations to catalyze the reaction (Chen and Morris, 1972a). An induction period may additionally imply a chain mechanism (Chen and Morris, 1972a; Millero, 1986) whereby the autocatalytic intermediates are continuously generated as the reaction proceeds at sufficient levels to sustain the reaction once it has begun. The likely autocatalytic intermediates are the reactive oxygen species (e.g., O_2^-, HO_2^-/H_2O_2) that may react with HS^- more readily with O_2 and may be

generated by numerous one and two electron transfer reactions as part of the overall sulfide autoxidation mechanism. The presence of an induction period also implies that the direct reaction of HS^- with O_2 is kinetically inhibited and proceeds slowly, consistent with many elementary (1–2 electron transfer) reactions between H_2S and O_2 being thermodynamically unfavorable (Luther, 2010; Luther et al., 2011).

Induction periods have been observed in some previous sulfide oxidation experiments (Chen and Morris, 1972a) but do not appear to be a consistently observed feature of the reaction. For example, induction periods are not reported in Millero et al. (1987), Vazquez et al. (1989), Zhang and Millero (1993a), or many other earlier experiments (including those performed in seawater at 10 °C; Cline and Richards, 1969). Chen and Morris (1972a) report induction periods over a wide range of experimental conditions (25 °C, pH = 6.0–11.75, $[H_2S_T]_{initial}$ = 50–200 μM, $[O_2]_{initial}$ = 160–800 μM) between 0.2 and 6 h that may roughly correlate inversely with the overall rate constant, which is generally consistent with our observations (Table 2). It is noteworthy that experiments performed at lower temperatures in previous studies (as low as 5–10 °C; Cline and Richards, 1969; Millero et al., 1987; Zhang and Millero, 1993a) were not reported to exhibit induction periods, because our experiments exhibited a pronounced induction period on the order of 1.5–2 days at 5 °C (Table 2; see also Supplementary Material).

The addition of trace levels of ferrous iron appears to decrease the induction period in our experiments (e.g., Fig. 1). As noted above, the catalytic cycle of ferrous iron likely involves the production of O_2^- and ferric iron, each of which are likely to be more effective oxidants towards sulfide than O_2 that may decrease the duration of an induction period. Trace metal catalysts such as ferrous iron have also been observed to decrease induction periods in sulfite (S^{4+}) oxidation experiments (e.g., see review in Brandt and van Eldik, 1995). It thus seems conceivable that induction periods may become undetectable upon sufficient level of catalysis (intentional or unintentional) (cf. Chen and Morris, 1972b). The lack of consistency in the observation of induction periods between experimental studies may be another feature of varying trace catalyst (metal or other) contaminations between laboratories and experimental approaches. Other than trace metals or other catalysts (e.g., organics), intermediate sulfur compounds (such as sulfite, elemental sulfur, or others) present in sulfide stock solutions may also influence the detection of induction periods by serving as autocatalysts either directly or indirectly (e.g., from their own more rapid oxidation under experimental conditions that may produce reactive oxygen species; Fig. 7).

4.4. Apparent break in rates in experiments with Fe^{2+} addition

Following a shortened induction period, our experiments where we added Fe^{2+} (~50–150 nM) to starting experimental solutions indicate that the reaction rate is increased (relative to our experiments where Fe^{2+} was not added) for a period of ca. 20–25 h before the reaction rate shifts to a value that is indistinguishable from our experiments where no Fe^{2+} was added (Fig. 1; Table 2). These observations suggest that the Fe^{2+} catalytic effect might be relatively short-lived when the supply of Fe^{2+} is finite. Zhang and Millero (1993a) observed similar behavior in sulfide oxidation experiments catalyzed by trace levels of Fe^{3+} (rather than Fe^{2+}) in seawater, finding that apparent rates returned to "background" levels from obviously catalyzed levels after only 30 min of reaction under their experimental conditions. They attributed this behavior to the formation of non-reactive colloidal forms of Fe^{3+} that can form over such short time scales. Zhang and Millero (1993a) argue that only dissolved forms of Fe^{3+} at trace-levels influence the rates of sulfide oxidation and colloidal ferric oxides may be ineffective as catalysts. Zhang and Millero (1991) also observed similar effects using both Fe^{2+} and Fe^{3+} as catalysts in sulfite (SO_3^{2-}) autoxidation experiments. Thus, the oxidation of Fe^{2+} in our experiments may have generated trace-levels of colloidal Fe^{3+} that built up over time such that ferric iron eventually could not effectively complete the catalytic cycle. If this hypothesis is correct, we might expect the timing of the break in rate to depend on the concentration of ferrous iron added but we do not appear to resolve any difference in the timing of the break over the ranges of ferrous iron that we investigated, which may suggest that the concentration dependence is subtle and/or our sampling interval was too course to observe such a difference. It is not clear why similar effects were not reported in previous Fe^{2+}-catalyzed sulfide oxidation experiments under high pH (Vazquez et al., 1989; Zhang and Millero, 1993a) but this may be due to the fact that these experiments went to completion in a matter of hours due to the ~10x lower initial concentrations of sulfide used than in the present study, and the reaction may have gone to completion before this effect could be observed.

The evolution of the isotopic composition of residual sulfide over the total duration of the monitored Fe^{2+}-catalyzed reactions (Fig. 3d and e) is consistent with a singular and invariant isotope effect despite the obvious break in rate approximately midway through the monitored reaction (Fig. 1). A shift in the magnitude of the fractionation factor corresponding to this break in rate might be expected because the break in rate implies a different operational mechanism for sulfide oxidation. It is likely that in order for this effect to be observed in our data the difference in the magnitude of the fractionation factor before and after the break in rate would have to be relatively large (i.e., greater than roughly ±1‰; see Supplementary Material), which apparently is not the case. The bulk of the isotope data corresponding to the ferrous iron catalyzed experiments was collected prior to the break in rate and may also be a reason for the lack of clear evidence for this observation.

4.5. Isotope fractionations: Comparison to previous studies

Fry et al. (1988) report $^{34}S/^{32}S$-based isotope enrichment factors ($^{34}\varepsilon_{P-R}$) for the autoxidation of sulfide in distilled

water (pH = 11) and artificial seawater (pH = 8.2) at 22–25 °C that were determined by tracking the isotopic composition of sulfide as a function of reaction progress as undertaken in the present study (Eq. (4)). The reported enrichment factors from Fry et al. (1988) yield values of $^{34}\varepsilon_{P-R} = -4.8 \pm 2.1‰$ in distilled water (3 experiments; 2 s.d.) and $^{34}\varepsilon_{P-R} = -5.8 \pm 5.2‰$ in artificial seawater (2 experiments, 2 s.d.). Thus, any difference in the measured enrichment factor as a function of pH and ionic strength over the studied range was not resolved. Their recommended value of $^{34}\varepsilon_{P-R} = -5.2 \pm 2.7‰$ (2 s.d.) is the average of all 5 experiments without error propagation. The rates of sulfide oxidation observed by Fry et al. (1988) cannot be placed into the context of the kinetics literature because they did not estimate rate constants from their experimental data. The value from the present study of $^{34}\varepsilon_{P-R} = -5.85 \pm 0.43‰$ (2 s.d., 2 experiments) from experiments conducted at 25 °C and pH = 9.8 is consistent with the measurements of Fry et al. (1988).

4.6. Major isotope discrimination as a function of rate: explicit catalysis and temperature

The explicitly Fe^{2+}-catalyzed experiments appear to yield isotope enrichment factors that are very similar to experiments where no Fe^{2+} was added (Figs. 4a and 5b, d). Experiments with $[Fe^{2+}]_{added} \sim 50$ nM exhibit increased reaction rates during the early portions of reactions (on the order of ~1.5 x faster) and an isotope enrichment factor ($^{34}\varepsilon_{P-R} = -5.63 \pm 0.65‰$, duplicate experiments, 2 s.d.) that is not resolvable from the experiments where no Fe^{2+} was added ($^{34}\varepsilon_{P-R} = -5.85 \pm 0.43‰$, duplicate experiments, 2 s.d.). The experiment with $[Fe^{2+}]_{added} \sim 150$ nM (~2x faster reaction rates initially) appears to exhibit a slightly lower enrichment factor ($^{34}\varepsilon_{P-R} = -4.90 \pm 0.23‰$, single experiment, 2 s.d.) that is not resolved from the $[Fe^{2+}]_{added} \sim 50$ nM experiments, but appears to be resolved from the experiments where no Fe^{2+} was added. If this apparent decrease in the magnitude of the fractionation factor from the studied conditions of $[Fe^{2+}]_{added} = 0$ to $[Fe^{2+}]_{added} \sim 150$ nM is a real feature of the studied reactions, then this observation may suggest that the pathways associated with ferrous iron catalysis (e.g., Eq. (18)) may be associated with slightly smaller magnitude isotope effects.

The isotope enrichment factors ($^{34}\varepsilon_{P-R}$) derived from experiments without ferrous iron added and performed as a function of temperature appear to exhibit a weak but potentially resolvable temperature dependence that if real is contrary to conventional expectation: fractionation magnitudes may increase with increasing temperature and increasing rate (Fig. 4a and b). The isotope enrichment factors derived from experiments performed at the end member temperatures (5 °C and 45 °C) are not resolvable from the 25 °C determinations but may be resolvable from one another (Fig. 4). If this is correct, we can envision a couple of hypothetical scenarios for this observation: (1) the HS⁻ species and its transition state with the principle reactant (i.e., reactive oxygen compound(s)) have high frequency and low frequency modes that compete (analogous to crossovers in equilibrium isotope exchange reactions; cf. Deines,

2003; Eldridge et al., 2016; or as invoked for vapor pressure isotope effects by Eiler et al., 2013), or (2) the rate determining steps are not the same at different temperatures, and are controlled by a different oxygen species at different temperatures (e.g., O_2 vs. O_2^- vs. O_2^{2-}) that have associated with them slightly different isotope effects, but this also has to be reconciled with the constant exponents of mass dependence (Fig. 5a). The latter possibility may be facilitated by different proportions and/or relative rates of the production of reactive oxygen species as part of the overall mechanism at different temperatures. However, the near constancy of $^{34}\varepsilon_{P-R}$ and $^{33/34}\theta$ may alternatively suggest very similar mechanisms of isotope fractionation over the studied temperature range.

4.7. Mass dependence of sulfide oxidation

By convention, the reference frame for evaluating the 'mass dependence' of any reaction or process based on multiple sulfur isotope ratio analysis is the mass dependence of equilibrium sulfur isotope exchange (cf. the definition of the $\Delta^{33}S$ and $\Delta^{36}S$ values, Eqs. (8) and (9). The principles governing the mass dependence of equilibrium isotope exchange among compounds are generally well understood. In the high temperature limit, the exponent of mass dependence for equilibrium isotope exchange reactions approaches a singular value for all compounds in a given isotope system that depends solely on the atomic masses (m) of the isotopes (Matsuhisa et al., 1978), e.g.:

$$\frac{\frac{1}{m_{32}} - \frac{1}{m_{33}}}{\frac{1}{m_{32}} - \frac{1}{m_{34}}} = 0.51588 \qquad (22)$$

$$\frac{\frac{1}{m_{32}} - \frac{1}{m_{36}}}{\frac{1}{m_{32}} - \frac{1}{m_{34}}} = 1.8904 \qquad (23)$$

At the low temperature limit, the exponent will vary depending on differences in the zero-point energies of the isotopologues (Matsuhisa et al., 1978) and the relationships between the reduced partition function ratios of the compounds considered (Eldridge et al., 2016). These differences influence the temperature dependence of the exponent and its value under the conditions relevant to low temperature aqueous systems. These variations have been theoretically estimated using quantum mechanical calculations for a variety of aqueous sulfur compounds and have been shown to follow systematic relationships that depend on the oxidation state of sulfur and its coordination to other atoms (Eldridge et al., 2016). For temperatures greater than 0 ° C, the $^{32}S/^{33}S/^{34}S$-based exponents derived from theoretical reduced partition function ratios (RPFRs) of aqueous sulfur compounds (spanning oxidation states of −2 to +6, and different structural configurations) conform to a relatively small range of ca. 0.5148–0.5159, and do not vary significantly outside the range of ~0.514–0.516 when translated into exponents associated with exchange reactions between two aqueous sulfur compounds (Eldridge et al., 2016). These calculations reveal that equilibrium isotope exchange exponents have potentially unique values for a given exchange reaction that will depend on the compound pair considered, but nevertheless fall within a

relatively narrowly defined range. A notable exception to this rule is where there are competitions from high and low frequency vibrational modes to RPFRs (cf. 'crossovers'; Deines, 2003; Eldridge et al., 2016), but these effects do not translate into substantial $\Delta^{33}S$ (or $\Delta^{36}S$) effects under equilibrium due to the very small isotope fractionations in proximity to crossover temperature. In short, the $^{33/34}\theta$ and $\Delta^{33}S_{P-R}$ values that we measure to be associated with sulfide oxidation (Fig. 5a and b) are not consistent with what we presently understand to be the values associated with equilibrium isotope exchange.

The direction of our measured $^{33/34}\theta$ and $\Delta^{33}S_{P-R}$ values (and possibly $^{36/34}\theta$ and $\Delta^{36}S_{P-R}$ values) is consistent with the simple hypothesis that unidirectional processes are associated with different mass laws. Young et al. (2002) (following Matsuhisa et al., 1978) argue that the mass-dependent fractionation laws of select irreversible processes may be different from those of equilibrium isotope exchange reactions. Utilizing considerations from both classical transition state theory (e.g., Bigeleisen, 1949) and Rice-Ramsperger-Kassel-Marcus (RRKM) theory (e.g., Marcus and Rice, 1951), Young et al. (2002) argue that certain unidirectional processes that are dominated by translations along the principle reaction coordinate (like evaporation and unimolecular dissociation reactions) should approach mass fractionation laws where:

$$^{n/34}\theta_{unidirectional} \approx \frac{\ln\left(\frac{m_{32}}{m_n}\right)}{\ln\left(\frac{m_{32}}{m_{34}}\right)} \quad (24)$$

where the 'm' can refer to atomic, molecular, or reduced masses of isotopic molecules depending on the process considered. At face value, these relationships can lead to $^{33/34}\theta$ exponents that are lower than those expected from equilibrium isotope exchange and $^{36/34}\theta$ exponents that are higher than those expected from equilibrium isotope exchange, roughly consistent with our experimental observations (Fig. 5a and c). For example, an exponent of $^{33/34}\theta = 0.50831$ is obtained from Eq. (24) if the atomic masses of sulfur are inputted, and similarly an exponent of $^{33/34}\theta = 0.50809$ is obtained if the molecular masses of HS^- are inputted, which are comparable to our experimental observations for sulfide autoxidation (Fig. 5a). Similarly, molecular masses for HS^- and atomic masses for S yield $^{36/34}\theta = 1.944–1.946$ that may also be comparable to our experimental observations (Fig. 5c).

Despite the apparent agreement between our measured exponents and the results of the application of Eq. (24), it is important to consider that the isotope fractionations associated with any given unidirectional process (and the 'mass dependence' thereof) are expected to be intrinsic properties of the reaction mechanism, and relations such as Eq. (24) do not take into consideration any particular aspects of a reaction mechanism. The simple form of Eq. (24) is only applicable to processes that involve reaction paths that can be assumed to be dominated by translational motions along the principle reaction coordinate, and therefore involve negligible contributions from the orthogonal vibrational modes of transition states. The isotope effects associated with the bimolecular electron transfer reactions involving multi-atomic transition states between sulfide compounds (HS^-) and oxygen species (e.g., O_2, O_2^-, O_2^{2-}) are likely to have contributions from the vibrational modes of transition states. Furthermore, even the simplest reaction path from reactant to and from transition state and ultimately to products involves mixing and transfer of isotopes between states, and this influences not only the fractionation but also the mass dependence. The explicit consideration of these states and their vibrational properties could be important in influencing the apparent mass law associated with sulfide autoxidation in a manner that is not accommodated by Eq. (24). A more accurate and applicable theoretical evaluation of the mass-dependence associated with sulfide autoxidation will likely require the explicit consideration of the principle transition states associated with sulfide autoxidation, and the consideration of any potentially other important reaction specific factors (e.g., isotopologue-specific transmissivity coefficients, and in principle the effects of tunneling that may not be significant for isotopologues of heavy elements like sulfur). These aspects of the sulfide autoxidation mechanism are not presently constrained but may be evaluated utilizing quantum mechanical software and various theories of unidirectional reactions in future studies.

Another alternative hypothesis is that the apparent shifts in the measured $^{n/34}\theta$ and $\Delta^n S_{P-R}$ are the result of so-called "mass conservation effects" and are related to the way that intermediates are linked in the reaction network (e.g., Farquhar et al., 2003). These effects are generally facilitated in a reaction network by reversible isotope exchange among compounds that have much different isotopic compositions and, thus, typically different oxidation states of sulfur. They have been documented in low temperature biological systems where reversible isotope exchange among sulfur compounds of different oxidation state seems to be mediated by the enzymes that are responsible for their intracellular transformation (e.g., Farquhar et al., 2003; Johnston et al., 2007). Such effects would require that sulfide autoxidation be at least a partially reversible process over the extent of reaction that we have studied (i.e., the residual sulfide must undergo reversible isotope exchange with some reaction intermediates in the early portions of the reaction network), and that the fractionation factor magnitudes between sulfide and the exchangeable intermediate be relatively large. At present, it is difficult to conceive of a plausible reverse exchange mechanism between residual sulfide and a product of sulfide autoxidation where the fractionation in terms of $^{34}\varepsilon$ between the two is large enough to generate the measured $^{n/34}\theta$ and $\Delta^n S_{P-R}$ effects. The intermediates that are likely to undergo reversible exchange are other reduced sulfur moieties such as the polysulfides (not analyzed in the present study) and possibly the reduced sulfur atom in thiosulfate (i.e., $S\text{-}SO_3^{2-}$; although the exchange kinetics with HS^- are not known over 5–45 °C and could be inhibitory), which are not presently understood to exhibit large fractionations with aqueous sulfide compounds. Additionally, the linearity of the Rayleigh plots (Fig. 3) is consistent with a singular and invariant isotope effect, and curvature in the trends plotted in Fig. 3 would be expected if reversibility were taking place that is not clearly resolved.

4.8. Implications: Potential signatures of sulfide autoxidation in the Cariaco Basin water column

Our observation that sulfide autoxidation appears to be accompanied by exponents of mass dependence (i.e., $^{33/34}\theta$) that are different at a resolvable level from ranges consistent with equilibrium isotope exchange (corresponding to small positive shifts in $\Delta^{33}S_{P-R}$ values) may enable the detection of a multiple sulfur isotope 'signature' for sulfide autoxidation in natural systems. One example is provided by the euxinic water column of the Cariaco Basin in the continental shelf of northeastern Venezuela (e.g., Li et al., 2010). The oxic-sulfidic interface in the Cariaco Basin at approximately ~260 m (2007–2008; Li et al., 2010) is marked by a depletion in the concentrations of dissolved oxygen from above and sulfide from below along with detectable concentrations of sulfur intermediates (SO_3^{2-}, $S_2O_3^{2-}$, and zero-valent sulfur) that have long been taken to be clear indications of the continual oxidation of sulfide (e.g., Fry et al., 1991; Zhang and Millero, 1993b; Li et al., 2010). The primary source of sulfide in the Cariaco water column is dissimilatory sulfate reduction that occurs in the underlying sediments and perhaps also in the water column (Li et al., 2010). The apparent sulfur isotope fractionation relationships observed between dissolved sulfide and sulfate in the deep waters of Cariaco are consistent with dissimilatory sulfate reduction occurring at relatively low rates (i.e., $^{34}\varepsilon_{sulfide-sulfate} = -54‰$, $^{33/34}\theta_{apparent} = 0.5127 \pm 0.0002$; Li et al., 2010; cf. Sim et al., 2011a, 2011b; cf. Leavitt et al., 2013). Evidence for contributions from organisms that disproportionate sulfur intermediates especially at/near the oxic-sulfidic interface have not been identified based on sulfur isotope analysis (cf. Li et al., 2010), and their contribution to sulfur cycling in Cariaco waters is not yet known.

Sulfide depletion in proximity to the oxic-sulfidic interface in Cariaco waters is associated with shifts in the sulfur isotope composition of dissolved sulfide. Li et al. (2010) observed a concomitant increase in the $\delta^{34}S$ value of aqueous sulfide with decreasing concentration of sulfide over depths of ~500–290 m that they observed to be consistent with the direction of the experimentally constrained isotope fractionations (based on $^{34}S/^{32}S$) associated with sulfide autoxidation (Fry et al., 1988) and chemotrophic sulfide oxidation associated with certain organisms (e.g., Kaplan and Rittenberg, 1964; Poser et al., 2014). Li et al. (2010) used a simple Rayleigh distillation model to infer the apparent enrichment factor associated with sulfide depletion throughout the water column (290–1300 m) of $^{34}\varepsilon_{P-R} = -1.1‰$, noting that this might be a minimum estimate of the fractionation magnitude due to the likely open-system behavior of the Cariaco Basin (we also note that if only data from 500 to 260 m depth are used where the increase in $\delta^{34}S$ is observed a slightly higher magnitude value of $^{34}\varepsilon_{P-R} = -1.8 \pm 0.5‰$ is obtained). However, Li et al. (2010) also observed a slight decrease in the $\Delta^{33}S$ value of aqueous sulfide that accompanies the increase in $\delta^{34}S$ that yields an apparent exponent of the fractionation associated with sulfide depletion of $^{33/34}\theta_{apparent} = 0.506 \pm 0.002$, which could not be completely explained by sulfide oxidation using the available constraints and therefore was taken

to be a potential indication of additional unknown processes occurring near or at the anoxic-oxic interface. We can now illustrate that the fractionation relationships in both $\delta^{34}S$ and $\Delta^{33}S$ ($^{33/34}\theta_{apparent}$) values in the Cariaco water column are consistent with sulfide autoxidation.

Using a simple Rayleigh model and the fractionations determined for sulfide autoxidation in the present study, we illustrate in Fig. 8 that the dissolved sulfide $\delta^{34}S$ and $\Delta^{33}S$ data (and perhaps $\Delta^{36}S$ data, although poorly resolved) in the water column of the Cariaco Basin are consistent with the experimental isotope fractionations associated with sulfide autoxidation. The predicted trajectory of the evolution of sulfide composition based on our experimentally-calibrated Rayleigh model indicates a slight but still resolvable decrease in $\Delta^{33}S$ that accompanies the increase in $\delta^{34}S$ that is indistinguishable from the apparent trajectory of the water column sulfide data of Li et al. (2010). The trajectory of the Rayleigh calculation in $\delta^{34}S$ vs. $\Delta^{33}S$ space in Fig. 8 does not appear to be sensitive to the magnitude of $^{34}\varepsilon_{P-R}$ up to values of approximately $-10‰$ (and is far more sensitive to $^{33/34}\theta$), and so the consistency between the Rayleigh fractionation trajectory and the Cariaco data persists in $\delta^{34}S$ vs. $\Delta^{33}S$ space despite the slightly larger magnitude experimental $^{34}\varepsilon_{P-R}$ associated with sulfide autoxidation (this study) than is apparent in the water column data of Li et al. (2010). For reference, we also display the results of a similar Rayleigh calculation using experimental data of phototrophic oxidation by green sulfur bacteria (Zerkle et al., 2009) that is expected to follow a different trajectory that is due primarily to the difference in the direction of the $^{34}\varepsilon_{P-R}$ of these two processes (as originally observed by Fry et al., 1988). As noted by Li et al. (2010), phototrophic oxidation is an unlikely contributor to sulfide oxidation in the Cariaco water column due to the lack of suitable light at these depths for phototrophic metabolism.

Experimental constraints for fractionation factors based on $^{33}S/^{32}S$, $^{34}S/^{32}S$, and $^{36}S/^{32}S$ do not exist for any other sulfide oxidation process at present including chemotrophic metabolisms, and so we cannot presently rule out other oxidation pathways in the Cariaco water column such as chemotrophic oxidation or abiological oxidation by other oxidants. Recently, Zerkle et al. (2016) reported analyses of the isotopic compositions ($\delta^{34}S$, $\Delta^{33}S$) of elemental sulfur and dissolved sulfide associated with biofilms in both fast-moving and stagnant waters in the Frasassi cave system that host natural populations of chemotrophic sulfide oxidizing organisms and inferred apparent isotope enrichment factors associated with the chemotrophic oxidation of sulfide to elemental sulfur. These data yield apparent fractionations in terms of $^{34}\varepsilon_{sulfur-sulfide(aq)}$ that range between $+8.43$ and $-0.9‰$ (Zerkle et al., 2016), where the bulk of the analyses (~32 out of the 37) yield positive apparent fractionations that would suggest an apparently inverse fractionation relationship between reactant sulfide and product S^0 that is analogous to phototrophic oxidation (e.g., Zerkle et al., 2009). The corresponding values of $\Delta^{33}S_{sulfur-sulfide(aq)}$ range between $+0.045$ to $-0.056‰$ ($^{33/34}\theta = 0.544–0.492$) and only a little over a third of the analyses indicate a value of $\Delta^{33}S_{sulfur-sulfide(aq)}$ that appears
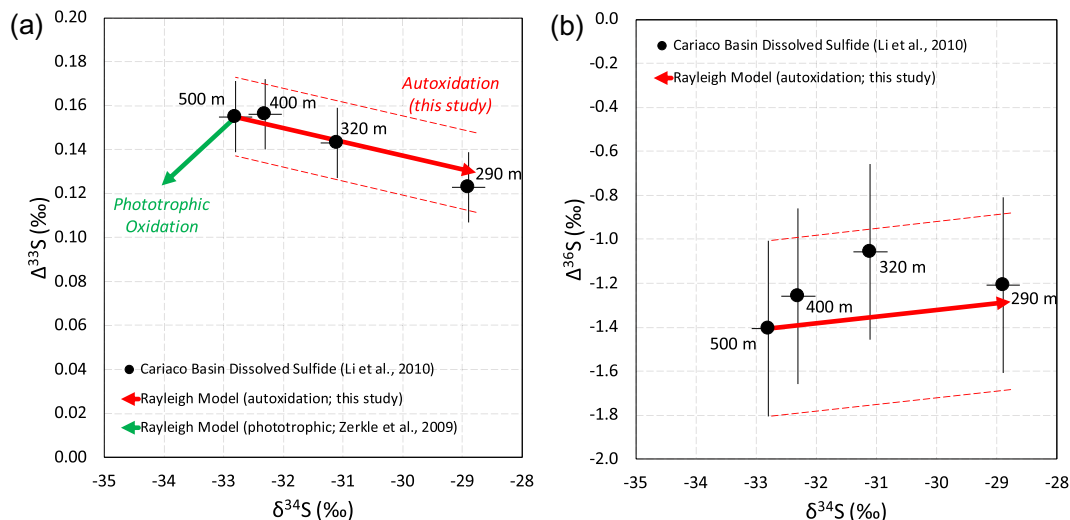
Fig. 8. The sulfur isotope compositions of dissolved water column sulfide in proximity to the oxic-anoxic(sulfidic) interface (located at ∼260 m depth at the time of sampling) in the Cariaco basin as reported in Li et al. (2010): (a) $\delta^{34}S$ vs. $\Delta^{33}S$, and (b) $\delta^{34}S$ vs. $\Delta^{36}S$ (all data reported in units of ‰). Lines indicate Rayleigh fractionation trajectories based on the experimental constraints for sulfide autoxidation (red; this study) and phototrophic oxidation by *Chlorobium tepidum* (green; Zerkle et al., 2009), where arrows indicate the direction of reaction progress (the corresponding dashed lines indicate estimated uncertainty, 2 s.d.). This analysis illustrates that as sulfide concentrations decrease in proximity to the oxic-anoxic interface due predominately to oxidation, the isotopic composition of sulfide follows a trajectory that is consistent with the experimental isotope fractionations constrained for sulfide autoxidation in the present study. (For interpretation of the references to colour in this figure legend, the reader is referred to the web version of this article.)

to be resolvable from zero based on their estimated analytical uncertainty of ±0.016‰ (2 s.d.) (Zerkle et al., 2016). For those samples that appear to have a resolvable $\Delta^{33}S_{sulfur-sulfide(aq)}$, the apparent $^{34}\varepsilon_{P-R}/\Delta^{33}S_{P-R}$ fractionation relationships in the biofilms are generally not consistent with autoxidation (this study, i.e.: $^{34}\varepsilon_{P-R}$ = negative, $\Delta^{33}S_{P-R}$ = positive, $^{33/34}\theta < 0.515$), but appear to be either qualitatively comparable to phototrophic oxidation (i.e., $^{34}\varepsilon_{P-R}$ = positive, $\Delta^{33}S_{P-R}$ = positive, $^{33/34}\theta > 0.515$; Zerkle et al., 2009) or are relatively unique (e.g., $^{34}\varepsilon_{P-R}$ = positive, $\Delta^{33}S_{P-R}$ = negative, $^{33/34}\theta < 0.515$; Zerkle et al., 2016). It thus remains unclear how the sulfur isotope fractionations compare between chemotrophic and other sulfide oxidation processes, and whether a role for microbial sulfide oxidation can be identified or distinguished in the Cariaco water column based on sulfur isotope data. Despite the present knowledge gap, our analysis may indicate that under certain circumstances a 'signature' of aqueous sulfide autoxidation may be apparent from the analysis of all three isotope ratios of dissolved sulfide in euxinic water columns, and the constraints in the present study will undoubtedly affect how sulfide autoxidation processes are treated in environmental models of the sulfur cycle based on all three sulfur isotope ratios.

5. CONCLUSIONS

We present the rates and multiple sulfur isotope fractionations associated with the oxidation of sulfide with molecular oxygen (autoxidation) as a function of temperature (5–45 °C) and ferrous iron catalysis ($[Fe^{2+}]_{added}$ = 50–150 nM). The second order rate constants (k) and apparent activation energy (E_a) that we derive from our experiments

generally compare well to previous experimental work. We additionally observe induction periods in our experiments that imply very slow initial reaction rates between HS^- and O_2 that have implications for the reaction mechanism. Major isotope enrichment factors ($^{34}\varepsilon_{P-R}$) derived from experiments conducted under all conditions are similar in magnitude and may exhibit subtle variations as a function of temperature and ferrous iron catalysis over the ranges we have investigated. Our values for $^{34}\varepsilon_{P-R}$ (e.g., -5.85 ± 0.43‰ at 25 °C; 2 s.d.) compare well to previous experimental observations (-5.2 ± 2.7‰ at 22-25 °C; Fry et al., 1988) in terms of both direction and magnitude, but we make the new observation that sulfide autoxidation under all conditions studied exhibits a mass dependence with respect to $^{33}S/^{32}S$ and $^{34}S/^{32}S$ relationships ($^{33/34}\theta$ and $\Delta^{33}S_{P-R}$) that is distinguishable from the range expected for equilibrium isotope exchange. The $^{36}S/^{32}S$ and $^{34}S/^{32}S$ relationships ($^{36/34}\theta$ and $\Delta^{36}S_{P-R}$) associated with sulfide autoxidation might also be different from equilibrium isotope exchange but such a difference is not resolved under all studied conditions. Differences in the mass-dependence of sulfide autoxidation as a function of oxidation rate associated with either ferrous iron catalysis or temperature are not resolved, and the mean values from all experiments yield: $^{33/34}\theta = 0.508 \pm 0.003$, $\Delta^{33}S_{P-R} = 0.037 \pm 0.014$‰, $^{36/34}\theta = 1.94 \pm 0.06$, and $\Delta^{36}S_{P-R} = -0.21 \pm 0.34$‰ (2 s.d., 7 experiments based on 38 isotopic analyses). These new experimental observations potentially enable the identification of a 'signature' for sulfide autoxidation in the isotopic composition of dissolved sulfide in the water column of the Cariaco basin in proximity to the oxic-sulfidic interface. The observation that sulfide autoxidation is associated with a mass dependence that is resolvable from equilibrium isotope

exchange changes our understanding of the isotope fractionations associated with the abiological sulfur cycling and will require updated treatment in future models of the sulfur cycle based on multiple sulfur isotope ratios.

ACKNOWLEDGEMENTS

REFERENCES

Almgren T. O. M. and Hagstrom I. (1974) The oxidation rate of sulphide in sea water. *Water Res.* **8**, 395–400.

Avrahami M. and Golding R. M. (1968) The oxidation of the sulphide ion at very low concentrations in aqueous solutions. *J. Chem. Soc. A Inorganic Phys. Theor.* **68**, 647–651.

Benson B. B. and Krause, Jr., D. (1980) The concentration and isotopic fractionation of gases dissolved in freshwater in equilibrium with the atmosphere. 1. Oxygen. *Limnol. Oceanogr.* **25**, 662–671.

Benson B. B. and Krause D. (1984) The concentration and isotopic fractionation of oxygen dissolved in freshwater and seawater in equilibrium with the atmosphere. *Limnol. Oceanogr.* **29**, 620–632.

Bigeleisen J. (1949) The relative reaction velocities of isotopic molecules. *J. Chem. Phys.* **17**, 675–678.

Bigeleisen J. and Wolfsberg M. (1958) Theoretical and experimental aspects of isotope effects in chemical kinetics. *Adv. Chem. Phys.* **1**, 15–76.

Bowles M. W., Mogollón J. M., Kasten S., Zabel M. and Hinrichs K.-U. (2014) Global rates of marine sulfate reduction and implications for sub-sea-floor metabolic activities. *Science* **344**, 889–891.

Brandt C. and van Eldik R. (1995) Transition metal-catalyzed oxidation of sulfur(IV) oxides. Atmospheric-Relevant Processes and Mechanisms. *Chem. Rev.* **95**, 119–190.

Canfield D. E. and Teske A. (1996) Late Proterozoic rise in atmospheric oxygen concentration inferred from phylogenetic and sulphur-isotope studies. *Nature* **382**, 127−.

Chen K. Y. and Morris J. C. (1972a) Kinetics of oxidation of aqueous sulfide by O2. *Environ. Sci. Technol.* **6**, 529–537.

Chen K. Y. and Morris J. C. (1972b) Oxidation of sulfide by O2: catalysis and inhibition. *J. Sanit. Eng. Div.* **98**, 215–227.

Clayton R. N. and Mayeda T. K. (1996) Oxygen isotope studies of achondrites. *Geochim. Cosmochim. Acta* **60**, 1999–2017.

Cline J. D. (1969) Spectrophotometric determination of hydrogen sulfide in natural waters. *Limnol. Oceanogr.* **14**, 454–458.

Cline J. and Richards F. (1969) Oxygenation of hydrogen sulfide in seawater at constant salinity, temperature and pH. *Environ. Sci. Technol.* **3**, 838–843.

Connick R. E. and Zhang Y.-X. (1996) Kinetics and mechanism of the oxidation of HSO3- by O2. 2. The manganese(II)-catalyzed reaction. *Inorg. Chem.* **35**, 4613–4621.

Connick R. E., Zhang Y.-X., Lee S., Adamic R. and Chieng P. (1995) Kinetics and mechanism of the oxidation of HSO3- by O2. 1. The uncatalyzed reaction. *Inorg. Chem.* **34**, 4543–4553.

Craig H. (1957) Isotopic standards for carbon and oxygen and correction factors for mass-spectrometric analysis of carbon dioxide. *Geochim. Cosmochim. Acta* **12**, 133–149.

Deines P. (2003) A note on intra-elemental isotope effects and the interpretation of non-mass-dependent isotope variations. *Chem. Geol.* **199**, 179–182.

Eiler J., Cartigny P., Hofmann A. E. and Piasecki A. (2013) Non-canonical mass laws in equilibrium isotopic fractionations: Evidence from the vapor pressure isotope effect of SF6. *Geochim. Cosmochim. Acta* **107**, 205–219.

Eldridge D. L., Guo W. and Farquhar J. (2016) Theoretical estimates of equilibrium sulfur isotope effects in aqueous sulfur systems: Highlighting the role of isomers in the sulfite and sulfoxylate systems. *Geochim. Cosmochim. Acta* **195**, 171–200.

Farquhar J., Johnston D. T., Wing B. A., Habicht K. S., Canfield D. E., Airieau S. and Thiemens M. H. (2003) Multiple sulphur isotopic interpretations of biosynthetic pathways: implications for biological signatures in the sulphur isotope record. *Geobiology* **1**, 27–36.

Fry B., Ruf W., Gest H. and Hayes J. M. (1988) Sulfur isotope effects associated with oxidation of sulfide by O2 in aqueous solution. *Chem. Geol.* **73**, 205–210.

Fry B., Jannasch H. W., Molyneaux S. J., Wirsen C. O., Muramoto J. A. and King S. (1991) Stable isotope studies of the carbon, nitrogen and sulfur cycles in the Black Sea and the Cariaco Trench. *Deep-Sea Res. A* **38**(S2), S1003–S1019.

Hershey J. P., Plese T. and Millero F. J. (1988) The pK1* for the dissociation of H2S in various ionic media. *Geochim. Cosmochim. Acta* **52**, 2047–2051.

Hoffmann M. R. and Lim B. C. (1979) Kinetics and mechanism of the oxidation of sulfide by oxygen: catalysis by homogeneous metal-phthalocyanine complexes. *Environ. Sci. Technol.* **13**, 1406–1414.

Johnston D. T., Farquhar J. and Canfield D. E. (2007) Sulfur isotope insights into microbial sulfate reduction: When microbes meet models. *Geochim. Cosmochim. Acta* **71**, 3929–3947.

Jørgensen B. B. (1977) The sulfur cycle of a coastal marine sediment (Limfjorden, Denmark). *Limn. Oceanog.* **22**, 814–832.

Jørgensen B. B. (1982) Mineralization of organic matter in the sea bed the role of sulphate reduction. *Nature* **296**, 643–645.

Jørgensen B. B., Bang M. and Blackburn T. H. (1990) Anaerobic mineralization in marine-sediments from the baltic-sea-north-sea transition. *Mar. Ecol. Ser.* **59**, 39–54.

Jørgensen B. B. and Nelson D. C. (2004) *Sulfide oxidation in marine sediments: Geochemistry meets microbiology*. GSA Special Papers, pp. 63–81.

Kaplan I. R. and Rittenberg S. C. (1964) Microbiological Fractionation of Sulphur Isotopes. *J. Gen. Microbiol.* **34**(2), 195–212.

Leavitt W. D., Halevy I., Bradley A. S. and Johnston D. T. (2013) Influence of sulfate reduction rates on the Phanerozoic sulfur isotope record. *Proc. Natl. Acad. Sci. U. S. A.* **110**, 11244–11249.

Li X., Gilhooly W. P., Zerkle A. L., Lyons T. W., Farquhar J., Werne J. P. and Scranton M. I. (2010) Stable sulfur isotopes in the water column of the Cariaco Basin. *Geochim. Cosmochim. Acta* **74**(23), 6764–6778.

Luther G. W. (2010) The role of one- and two-electron transfer reactions in forming thermodynamically unstable intermediates as barriers in multi-electron redox reactions. *Aquat. Geochem.* **16**, 395–420.

Luther G. W., Findlay A. J., MacDonald D. J., Owings S. M., Hanson T. E., Beinart R. A. and Girguis P. R. (2011) Thermodynamics and kinetics of sulfide oxidation by oxygen: A look at inorganically controlled reactions and biologically mediated processes in the environment. *Front. Microbiol.* **2**, 1–9.

Marcus R. A. and Rice O. K. (1951) The kinetics of the recombination of methyl radicals and iodine atoms. *J. Phys. Colloid Chem.* **55**, 894–908.

Mariotti A., Germon J. C., Hubert P., Kaiser P., Letolle R., Tardieux A. and Tardieux P. (1981) Experimental determination of nitrogen kinetic isotope fractionation: Some principles; illustration for the denitrification and nitrification processes. *Plant Soil* **62**, 413–430.

Matsuhisa Y., Goldsmith J. R. and Clayton R. N. (1978) Mechanisms of hydrothermal crystallization of quartz at 250° C and 15 kbar. *Geochim. Cosmochim. Acta* **42**, 173–182.

Miller M. F. (2002) Isotopic fractionation and the quantification of 17O anomalies in the oxygen three-isotope system: An appraisal and geochemical significance. *Geochim. Cosmochim. Acta* **66**, 1881–1889.

Millero F. J. (1991a) The oxidation of H2S in the Chesapeake Bay. *Estuar. Coast. Shelf Sci.* **33**, 521–527.

Millero F. J. (1991b) The oxidation of H2S in Black Sea waters. *Dee-Sea Res.* **38**, S1139–S1150.

Millero F. J. (1991c) The oxidation of H2S in Framvaren Fjord. *Limnol. Oceanogr.* **36**, 1007–1014.

Millero F. J. (1986) The thermodynamics and kinetics of the hydrogen sulfide system in natural waters. *Marine Chem.* **18**, 121–147.

Millero F. J., Hubinger S., Fernandez M. and Garnett S. (1987) Oxidation of H2S in seawater as a function of temperature, pH, and ionic strength. *Environ. Sci. Tech.* **21**, 439–443.

Millero F. J., Leferriere A., Fernander M., Hubinger S. and Hershey J. P. (1989) Oxidation of H2S with H2O2 in natural waters. *Environ. Sci. Technol.* **23**(2), 209–213.

O'Brien D. J. and Birkner F. B. (1977) Kinetics of oxygenation of reduced sulfur species in aqueous solution. *Environ. Sci. Technol.* **11**, 1114–1120.

Ostlund H. G. and Alexander J. (1963) Oxidation rate of sulfide in sea water, a preliminary study. *J. Geophys. Res.* **68**, 3995–3997.

Poser A., Vogt C., Knöller K., Ahlheim J., Weiss H., Kleinsteuber S. and Richnow H. H. (2014) Stable sulfur and oxygen isotope fractionation of anoxic sulfide oxidation by two different enzymatic pathways. *Environ. Sci. Technol.* **48**(16), 9094–9102.

Scott K. M., Lu X., Cavanaugh C. M. and Liu J. S. (2004) Optimal methods for estimating kinetic isotope effects from different forms of the Rayleigh distillation equation. *Geochim. Cosmochim. Acta* **68**, 433–442.

Sim M. S., Bosak T. and Ono S. (2011a) Large sulfur isotope fractionation does not require disproportionation. *Science* **333**, 74–77.

Sim M. S., Ono S., Donovan K., Templer S. P. and Bosak T. (2011b) Effect of electron donors on the fractionation of sulfur isotopes by a marine Desulfovibrio sp. *Geochim. Cosmochim. Acta* **75**, 4244–4259.

Tossell J. A. (1997) Theoretical studies on possible sulfur oxides with +2 oxidation states in aqueous solution. *Chem. Geol.* **141**, 93–103.

Vairavamurthy M. A. and Zhou W. (1995) Characterization of a transient +2 sulfur oxidation state intermediate from the oxidation of aqueous sulfide. In *Geochemical Transformations of Sedimentary Sulfur* (eds. M. A. Vairavamurthy and M. A. A. Schoonen). American Chemical Society, Washington, D.C., pp. 280–292.

Vazquez F., Zhang J.-Z. and Millero F. J. (1989) Effect of metals on the rate of the oxidation of H2S in seawater. *Geophys. Res. Lett.* **16**, 1363–1366.

Young E. D., Galy A. and Nagahara H. (2002) Kinetic and equilibrium mass-dependant isotope fractionation laws in nature and their geochemical and cosmochemical significance. *Geochim. Cosmochim. Acta* **66**, 1095–1104.

Zerkle A. L., Farquhar J., Johnston D. T., Cox R. P. and Canfield D. E. (2009) Fractionation of multiple sulfur isotopes during phototrophic oxidation of sulfide and elemental sulfur by a green sulfur bacterium. *Geochim. Cosmochim. Acta* **73**, 291–306.

Zerkle A. L., Jones D. S., Farquhar J. and Macalady J. L. (2016) Sulfur isotope values in the sulfidic Frasassi cave system, central Italy: A case study of a chemolithotrophic S-based ecosystem. *Geochim. Cosmochim. Acta* **173**, 373–386.

Zhang J.-Z. and Millero F. J. (1991) The rate of sulfite oxidation in seawater. *Geochim. Cosmochim. Acta* **55**, 677–685.

Zhang J.-Z. and Millero F. J. (1993a) The products from the oxidation of H₂S in seawater. *Geochim. Cosmochim. Acta* **57**, 1705–1718.

Zhang J. Z. and Millero F. J. (1993b) The chemistry of the anoxic waters in the Cariaco Trench. *Deep-Sea Res. Part I* **40**(5), 1023–1041.

Zopfi J., Ferdelman T. G. and Fossing H. (2004) *Distribution and fate of sulfur intermediates—sulfite, tetrathionate, thiosulfate, and elemental sulfur—in marine sediments*. GSA Special Papers, pp. 97–116.

Associate editor: Timothy Lyons